NEUROSCIENCE

TRPM7 kinase activity induces amyloid-β degradation to reverse synaptic and cognitive deficits in mouse models of Alzheimer's disease

Shimeng Zhang†, Feifei Cao†, Wei Li*, Nashat Abumaria*

Altered abundance or activity of the dual-function transient receptor potential melastatin-like 7 (TRPM7) protein is implicated in neurodegenerative disorders, including Alzheimer's disease (AD). Toxic aggregation of amyloid-β (Aβ) in neurons is implicated in AD pathology. Here, we found that the kinase activity of TRPM7 is important to stimulate the degradation of Aβ. TRPM7 expression was decreased in hippocampal tissue samples from patients with AD and two mouse models of AD (*APP/PS1* and *5XFAD*). In cultures of hippocampal neurons from mice, overexpression of full-length TRPM7 or of its functional kinase domain M7CK prevented synapse loss induced by exogenous Aβ. In contrast, this neuroprotection was not afforded by overexpression of either the functional ion channel portion alone or a TRPM7 mutant lacking kinase activity. M7CK overexpression in the hippocampus of young and old *5XFAD* mice prevented and reversed, respectively, memory deficits, synapse loss, and Aβ plaque accumulation. In both neurons and mice, M7CK interacted with and activated the metalloprotease MMP14 to promote Aβ degradation. Thus, TRPM7 loss in patients with AD may contribute to the associated Aβ pathology.

INTRODUCTION

Alzheimer's disease (AD) is a neurodegenerative disorder characterized by amyloid-β (Aβ) deposition, synapse loss, and cognitive impairments (*1*–*3*). Aβ deposition is regulated by the balance between Aβ production and clearance (*4*). One hallmark of AD pathology is alterations in the Aβ production and clearance rate, resulting in the accumulation of Aβ and other toxic peptides in the brain (*5*, *6*). Synapse loss is another hallmark of AD pathology that is also linked to cognitive decline (*3*, *7*, *8*). Thus, reducing Aβ accumulation or maintaining synaptic density may preserve normal cognitive functions in patients with AD.

Aβ clearance is partly mediated by Aβ-degrading enzymes that include insulin-degrading enzyme (IDE), neprilysin (NEP), angiotensin-converting enzyme (ACE), and various matrix metalloproteinases (MMPs) (*9*). MMPs are zinc-containing endopeptidases involved in Aβ degradation, synaptic functions, and cell motility (*10*). In patients with AD, *MMP14* mRNA levels are up-regulated in the temporal cortex (*11*). MMP14 protein expression is increased in the hippocampi of *5XFAD* mice, an experimental animal model (*12*). An increase in MMP14 expression promotes Aβ degradation in astrocytes (*11*). Thus, the Aβ-degrading enzyme MMP14 may play a role in AD pathology and could be a potential therapeutic target to reduce Aβ plaques, protect synapses, and prevent memory deficits.

The transient receptor potential melastatin-like 7 (TRPM7) "channel enzyme" is a unique ion channel in that it contains a kinase domain in its C terminus (*13*, *14*) that, when cleaved, translocates to the nucleus to regulate various cellular functions (*15*). In the mammalian brain, the cleaved kinase domain is important for synaptic density, synaptic plasticity, and learning and memory (*16*). Some studies suggest that overexpression or increased activation of TRPM7 contributes to the pathologies of neurodegenerative disorders and, hence, that its suppression or inhibition represents a therapeutic strategy (*17*). In contrast, various other studies show that mutations in TRPM7 are associated with the neurodegenerative disorder Western Pacific amyotrophic lateral sclerosis and parkinsonism-dementia complex (*18*), that activation of TRPM7 decreases Aβ levels in cultured cell lines (*19*–*21*), and that TRPM7 or its kinase domain are critical for normal synaptic and cognitive functions (*16*, *22*, *23*). Thus, reductions in TRPM7 activity or expression could also contribute to pathologies of neurodegenerative disorders.

Here, we examined whether AD-like pathology in mouse models is associated with changes in TRPM7 expression and tested the hypothesis that rescuing the expression of the channel and/or the kinase domain (hereafter M7CK) could counteract Aβ pathology. We uncovered mechanistic insight into how M7CK can reduce Aβ plaques, protect synapses, and prevent memory deficits in *5XFAD* mice.

RESULTS

TRPM7 expression is down-regulated in the brains of patients with AD and two mouse models of AD

To determine TRPM7 expression during AD pathology, we quantified TRPM7 protein levels in postmortem brain tissues from six patients with AD and five healthy controls (table S1, and further detailed in Materials and Methods). We found that TRPM7 protein expression was significantly reduced in the hippocampi of patients with AD (Fig. 1A; also data file S1 and tables S2 to S4). *TRPM7* mRNA in these samples was also significantly reduced in the hippocampi of patients with AD (Fig. 1B).

The *5XFAD* mouse model of AD coexpresses five mutations linked to familial AD. These mice develop Aβ plaques, show synapse loss, and exhibit memory deficits before 6 months of age

State Key Laboratory of Medical Neurobiology and MOE Frontiers Center for Brain Science, Institutes of Brain Science, Fudan University, Shanghai 200032, China.
*Corresponding author. Email: abumaria@fudan.edu.cn (N.A.); leewei@fudan.edu.cn (W.L.)
†These authors contributed equally to this work.

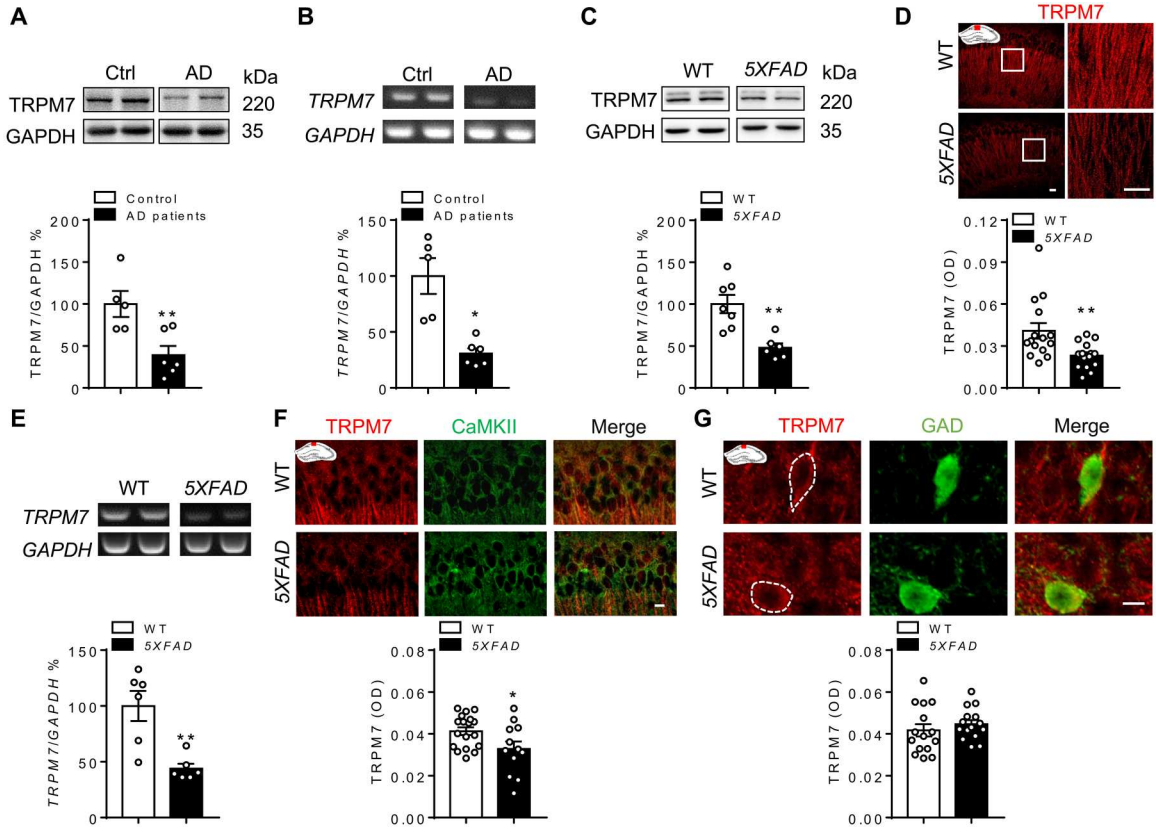

Fig. 1. Reduced expression of TRPM7 mRNA and protein in the hippocampus of patients with AD and *5XFAD* mice. (**A**) Representative Western blots and quantitative analysis of TRPM7 protein in the hippocampi of patients with AD ($n = 6$) and healthy controls ($n = 5$). Density of TRPM7 protein bands were normalized to GAPDH and then calculated as a percentage of control group. The co-detection of GAPDH bands served as loading control. Data were analyzed by an unpaired *t* test. (**B**) Representative bands and quantitative analysis of *TRPM7* mRNA in the hippocampi of patients with AD ($n = 6$) and healthy controls ($n = 5$). GAPDH bands served as loading control. Data were analyzed by an unpaired *t* test with Welch's correction. (**C**) Assay and analysis described in (A), from the hippocampi of WT ($n = 7$) and *5XFAD* ($n = 6$) mice at the age of 12 months. Data were compared by unpaired *t* test. (**D**) Top: Representative fluorescent images of TRPM7 immunostaining and an illustration of the CA1 region in which images were taken and analyzed. Bottom: Quantitative analysis of the optical density (OD) of TRPM7 in the striatum radiatum of the CA1 from WT and *5XFAD* mice at the age of 12 months ($n = 15$ brain sections from five mice per group). Mann-Whitney test. Scale bar, 30 μm. (**E**) As described in (B), from the hippocampi of WT ($n = 6$) and *5XFAD* ($n = 6$) mice at the age of 12 months. Data were analyzed by Mann-Whitney test. (**F**) Top: Representative fluorescent images of TRPM7 (red) and CaMKII (green). Bottom: Quantitative analysis of TRPM7 optical density in cell body of CaMKII positive neurons in the CA1 areas of WT ($n = 18$ brain sections from six mice) and *5XFAD* ($n = 12$ brain sections from four mice) mice at the age of 12 months. Data were analyzed by an unpaired *t* test. Scale bar, 20 μm. (**G**) As described in (F), but for the quantitative analysis of TRPM7 optical density in the cell body of GABAergic neurons. $N = 15$ brain sections from five mice per group, analyzed by unpaired *t* test. Scale bar, 10 μm. For each mouse, three brain sections were used for immunofluorescent quantitative analysis. $^*P < 0.05$ and $^{**}P < 0.01$ by the test specified, with further details in tables S2 to S4, and full-length Western blots in data file S1.

(*24*). We quantified TRPM7 protein expression in the hippocampi of *5XFAD* mice at the age of 12 months and found that TRPM7 protein expression was significantly reduced in these mice compared with wild-type (WT) mice (Fig. 1C). These results were confirmed by using quantitative immunohistochemistry analysis of hippocampal sections obtained from *5XFAD* mice of the same age (Fig. 1D). We also found that *TRPM7* mRNA was significantly reduced in these *5XFAD* mice (Fig. 1E). Similar observations were obtained by using brain samples from another widely used mouse model of AD, namely, the *APP/PS1* mouse model, which coexpresses two familial AD–linked mutations and shows Aβ deposits and memory impairments before 8 months of age (*25*, *26*). Using quantitative Western blotting and immunohistochemistry, we found that TRPM7 protein expression was significantly reduced in the hippocampi of *APP/PS1* mice at the ages of 15 and 19 months (fig. S1, A and B). It is worth noting that the observed reductions in TRPM7 expression in *5XFAD* and *APP/PS1* mice were not due to cell loss within the hippocampus. We found that the estimated total cell density and neuronal density within the CA1 region in *5XFAD* (fig. S1C) and *APP/PS1* (fig. S1D) mice was similar to that in the WT mice. TRPM7 protein expression was down-regulated in calcium/calmodulin-dependent kinase II (CaMKII)–positive glutamatergic neurons (Fig. 1F) but not in glutamic acid decarboxylase 67 (GAD67)–positive GABAergic neurons (Fig. 1G). These data suggest that AD or AD-like pathology is associated with the down-regulation of TRPM7 expression. In agreement with previous findings in brain tissues from patients with AD (*27*), our data suggest that this down-regulation of TRPM7 occurred at the transcriptional level. Furthermore, our results demonstrate that AD-like pathology might result in reduction of TRPM7 expression within hippocampal glutamatergic neurons.

Overexpression of M7CK prevents Aβ-induced synapse loss in neuronal cultures

Our previous data show that deletion of *TRPM7* or suppression of its expression in glutamatergic neurons results in synapse loss, synaptic plasticity deficits, and memory impairments that can be reversed by overexpression of the kinase domain of TRPM7 (M7CK) (*16*). Here, we found that AD-like pathology in mice was associated with reductions in TRPM7 expression and that the decreases in TRPM7 expression mainly occurred in glutamatergic neurons. These changes might contribute to the synaptic and cognitive deficits associated with AD in patients. Therefore, we hypothesized that overexpressing the kinase domain might help rescue synaptic and cognitive deficits associated with AD-like pathology. Next, we tested this hypothesis in vitro and in vivo.

Increasing the extracellular concentration of $A\beta_{1–42}$ reduces the synaptic density in primary neuronal cultures (*28*). We tested whether overexpression of the C-terminal part of TRPM7, which was previously shown to be cleaved and carry the functional kinase domain (M7CK, amino acids 1299 to 1862) (*15*, *16*), can prevent the detrimental effects of Aβ on synaptic density. We found that 48 hours of incubation with Aβ resulted in significant reductions in the numbers of synaptophysin and PSD-95 puncta that was rescued by overexpression of M7CK (Fig. 2, A and B). In contrast, overexpressing an inactive mutant kinase (M7CK-K1646R) (*29*) failed to rescue the number of synaptophysin puncta (Fig. 2A), indicating that the kinase activity of M7CK is necessary to counteract Aβ toxicity in neuronal cultures. We also investigated whether, like the free M7CK and/or the cleaved kinase domain, a cytoplasm/cell membrane–enriched M7CK can rescue the synaptic density. We overexpressed an active form of M7CK with glycosylphosphatidylinositol (GPI) on each side to ensure that the kinase domain will be enriched on cell membrane or in the cytoplasm but not in the nucleus (fig. S2). We found that overexpressing M7CK outside the nucleus also rescued the change in the synaptic density induced by high extracellular Aβ concentrations (Fig. 2C), supporting the notion that the M7CK effects might be mediated by mechanisms other than chromatin or transcriptional modifications that were reported before in cell cultures (*15*). Overexpression of a truncated form of the TRPM7 ion channel (T7ΔK, amino acids 1 to 1510), which lacks the kinase domain but is a functional channel (*30*), failed to prevent the detrimental effects of Aβ on synaptic density (Fig. 2D). We further confirmed the protective effects of the kinase domain by using full-length TRPM7 overexpression (such that enzyme cleavage is under cell control). We found that overexpression of WT full-length TRPM7 or a full-length channel-deficient mutant [P1040R (*31*)] prevented the negative effect of Aβ on synaptic density in neuronal cultures. In contrast, overexpressing a kinase-deficient [K1646R (*29*)] full-length TRPM7 failed to prevent the negative effect of Aβ on synaptic density (Fig. 2E). Therefore, overexpressing TRPM7 kinase domain prevented the negative effect of Aβ on synaptic density in neuronal cultures. This protective effect against Aβ toxicity appeared to be dependent on the kinase activity of TRPM7 but independent of its cleavage status.

Overexpression of M7CK in the hippocampus rescues memory functions in *5XFAD* mice

Next, we tested whether overexpressing M7CK in the hippocampus can reverse memory deficits in the *5XFAD* mouse model. We bilaterally injected a group of WT mice with AAV-CAG-M7CK-EGFP (enhanced green fluorescent protein) to achieve sporadic expression of M7CK in the hippocampus and performed immunohistochemistry analysis to detect the M7CK-EGFP signal. We found that the M7CK-EGFP signal was enriched in or colocalized with CaMKII signal (a marker of glutamatergic neurons) (fig. S3A and data file S2), whereas colocalization with GAD65/67 (a marker of GABAergic neurons), ionized calcium-binding adaptor molecule 1 (IBA1; a marker of microglial cells), or glial fibrillary acidic protein (GFAP; a marker of astrocytes) was weaker (fig. S3, B to D).

Then, we injected AAV-CAG-EGFP or AAV-CAG-M7CK-EGFP bilaterally into the hippocampi of WT and *5XFAD* mice at the age of 5 months. One month later, we evaluated social behavior as well as learning and memory abilities (Fig. 3A). At the age of 6 months, the nesting behavior of *5XFAD* mice was impaired. Overexpression of M7CK in the hippocampi of *5XFAD* mice failed to prevent the impairment in nesting behavior (Fig. 3B). Using the novel object recognition test (NORT), we evaluated the mice′s memory. In contrast to WT mice, *5XFAD* mice showed no preference for the novel object during the 24-hour memory test. Similar to WT mice, *5XFAD* mice with hippocampus-specific overexpression of M7CK showed a significant preference for the novel object (Fig. 3C). We also evaluated the spatial learning and memory of the mice by using the cognition wall task. In this task, impairment of learning ability was observed in *5XFAD* mice compared with WT mice, and *5XFAD* mice overexpressing M7CK had a significantly faster learning rate than *5XFAD* mice (Fig. 3D). More than 84% of *5XFAD* mice overexpressing M7CK learned the task successfully. However, only 46% of *5XFAD* mice learned the task (Fig. 3D).

We next tested the duration of the effect of M7CK overexpression. To this end, we evaluated the cognitive functions of the same groups of mice at 10 and 15 months of age (Fig. 3, E to J). At these ages, *5XFAD* mice exhibited impairment of nesting behavior. Overexpression of M7CK in the hippocampi of *5XFAD* mice rescued nest construction scores at the age of 10 months but not at 15 months (Fig. 3, E and H). The *5XFAD* mice exhibited clear impairments in the 24-hour NORT memory tests (Fig. 3, F and I), and overexpression of M7CK rescued these memory impairments in *5XFAD* mice at the ages of 10 and 15 months (Fig. 3, F and I). Last, because the cognition wall task cannot be reliably used to study cognition multiple times in the same mice, we instead used the Y-maze to evaluate the spatial working memory of the mice. At both ages, *5XFAD* mice exhibited impairment of working memory (Fig. 3, G and J). *5XFAD* mice overexpressing M7CK in the hippocampus exhibited significantly better performance in the working memory trial of the Y-maze test at the ages of 10 and 15 months (Fig. 3, G and J).

It is worth noting that the total distance traveled in the open area and the total number of object exploration were similar for all animals from all groups (fig. S4, A to F). Thus, the observed differences in behavior were not due to changes in overall locomotor and/or exploratory activities. Furthermore, we did not observe any changes in behavioral scores between WT mice overexpressing M7CK and WT mice (Fig. 3, B to J). These observations suggest that M7CK overexpression counteracts AD-like pathology and that the kinase domain is not just a general synaptic and cognitive enhancer. Therefore, overexpression of M7CK can durably prevent impairment of learning and memory functions in *5XFAD* mice.

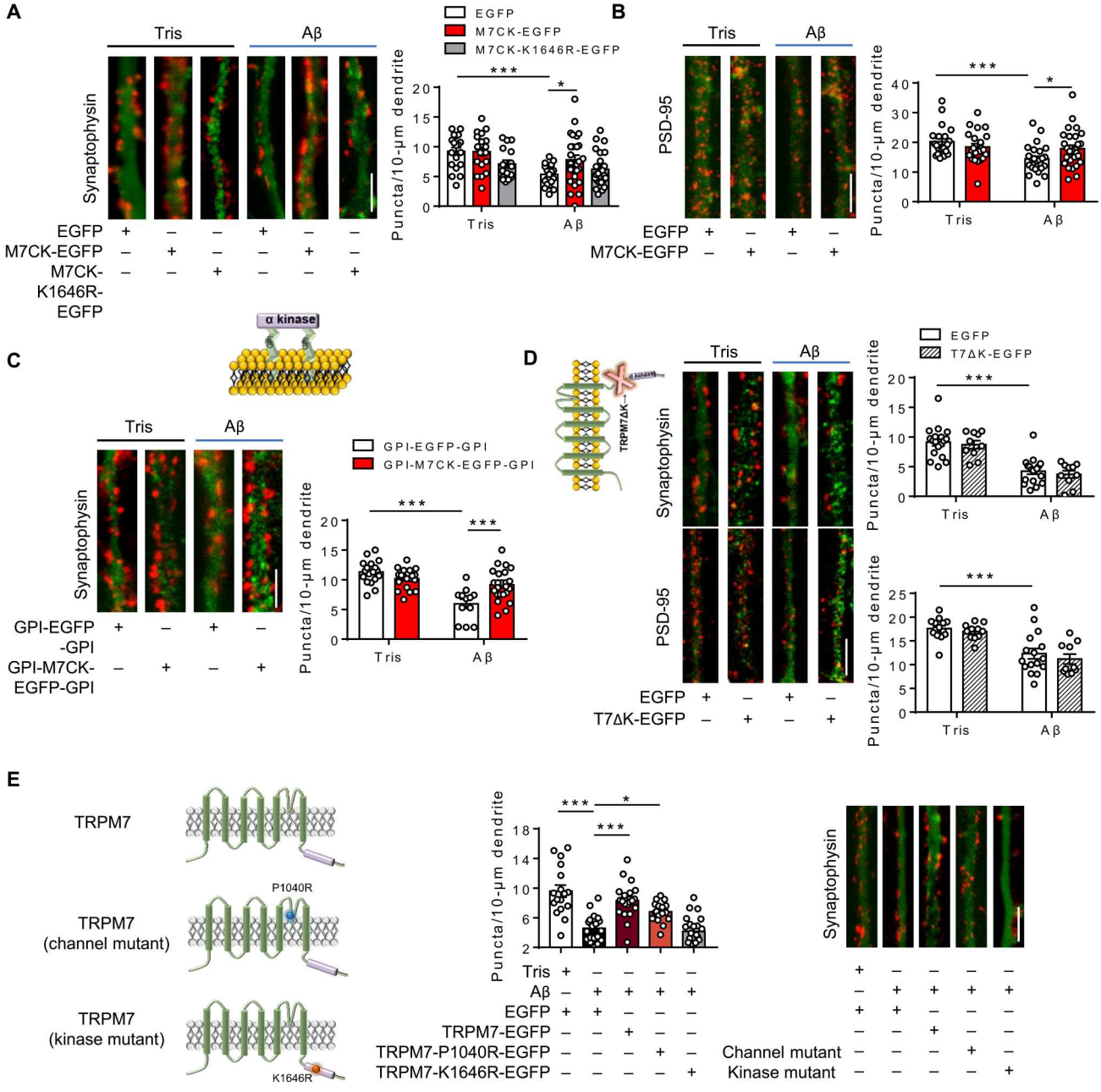

Fig. 2. Overexpression of the active kinase domain of TRPM7 prevents Aβ-induced toxicity on synapse density in hippocampal neuronal cultures. (**A**) Left: Fluorescent images of synaptophysin puncta in hippocampal neuronal cultures incubated with tris buffer or Aβ and transduced with AAV-EGFP, AAV-M7CK-EGFP, or AAV-M7CK-K1646R-EGFP virus. Right: Quantitative analysis of synaptophysin puncta density (minimum 16 neurons per group). (**B**) Same as (A), but for PSD-95 puncta (minimum 22 neurons per group). (**C**) Same as (A), but cultures were transduced with kinase domain that has two GPI anchors (AAV-GPI-M7CK-EGFP-GPI virus) (minimum 12 neurons per group). Illustration of the kinase domain with the GPI anchors is shown above. (**D**) Same as (A) and (B), but cultures were transduced with the truncated TRPM7 ion channel (TRPM7ΔK-EGFP) (minimum 10 neurons per group). Illustration of TRPM7 ion channel is shown. (**E**) Same as (A), but cultures were transfected with EGFP, TRPM7-EGFP, TRPM7-P1040R-EGFP, or TRPM7-K1646R-EGFP plasmid. Illustration of WT TRPM7, TRPM7 with channel mutant, and TRPM7 with kinase mutant is shown in left. In (A) to (E), *N* = at least 17 neurons per group, analyzed by one-way ANOVA followed by Bonferroni's post hoc test (E) or two-way ANOVA followed by Bonferroni's post hoc test for all others. Scale bar, 5 μm. All neurons were collected from three independent neuronal cultures. **P* < 0.05 and ****P* < 0.001 by the test specified, with further details in tables S3 and S4.

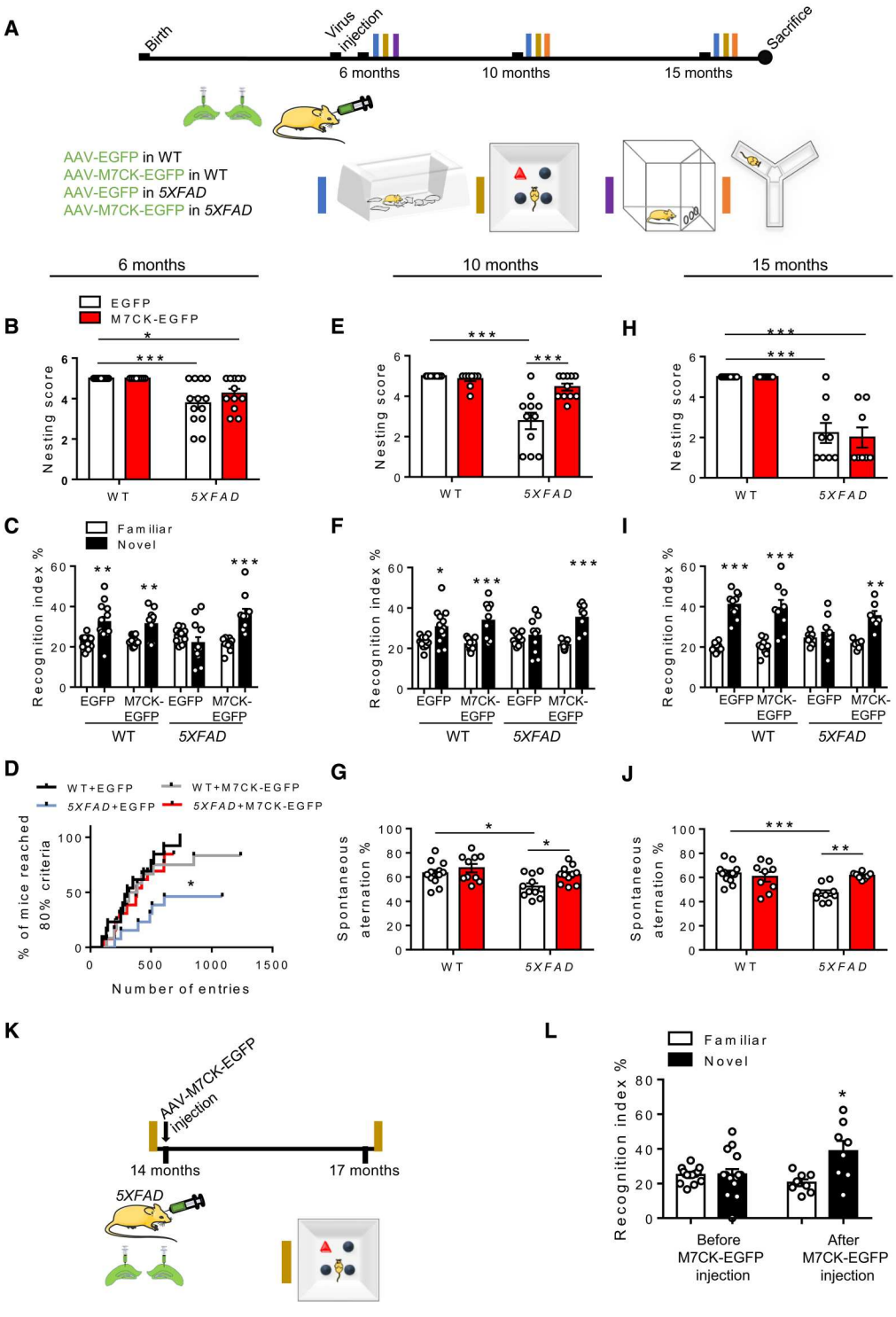

Fig. 3. Overexpression of M7CK in the hippocampus of *5XFAD* mice rescues/reverses memory deficits. (**A**) Schematic illustration of experimental design showing bilateral injections of AAV-EGFP or AAV-M7CK-EGFP virus in the hippocampus WT and *5XFAD* mice at the age of 5 months. Behavioral experiments were performed on the mice at the age of 6, 10, and 15 months. (**B**) Nesting scores of the mice during nesting construction social behavior at the age of 6 months. *N* = at least 12 mice per group, analyzed by two-way ANOVA followed by Bonferroni's post hoc test. (**C**) Recognition index of the novel object and that of the other three identical familiar objects (averaged) in the mice during NORT 24-hour memory test. *N* = at least 10 mice per group, analyzed by unpaired *t* test with Welch's correction. (**D**) Percentage of mice that successfully learned the cognition wall task during the 13 hours of spontaneous learning. *N* = at least 12 mice per group, analyzed by log-rank Mantel-Cox test. (**E** and **F**) Assays and statistical analyses are the same as described and from the same groups of animals in (B) and (C), respectively, but at the age of 10 months. *N* = at least 10 mice per group. (**G**) Spontaneous alternation (as percentage) during the Y-maze spatial working memory task in the same groups of 10-month-old animals as in (E) and (F). *N* = at least 10 mice per group, analyzed by two-way ANOVA followed by Bonferroni's post hoc test. (**H** and **I**) Assays and statistical analyses are the same as described and from the same groups of animals in (B) and (C) but at the age of 15 months. *N* = at least 7 (I) or 8 (H) mice per group. (**J**) As described in (G) and in the same groups of animals but at the age of 15 months. *N* = at least 8 mice per group, analyzed as in (G). (**K**) Schematic illustration of experimental design showing bilateral injections of AAV-M7CK-EGFP virus into the hippocampus of *5XFAD* mice at the age of 14 months. NORT was performed on the mice at 14 months (before M7CK-EGFP injection) and 17 months (after M7CK-EGFP injection). (**L**) Recognition index of the novel object and that of the other three identical familiar objects (averaged) during the 24-hour NORT memory test with *5XFAD* mice before and after M7CK-EGFP overexpression. *N* = at least 8 mice per group, analyzed by unpaired *t* test with Welch's correction. **P* < 0.05, ***P* < 0.01, and ****P* < 0.001 by the test specified, with further details in tables S2 to S4.

The data thus far suggest that M7CK overexpression at early time points can prevent memory impairment during AD-like pathology. To investigate whether M7CK overexpression can restore memory functions in aging and cognitively impaired mice, we evaluated memory function in a separate group of male and female *5XFAD* mice at the age of 14 months. Then, we overexpressed M7CK in their hippocampi and reevaluated the memory functions of the same animals at the age of 17 months (those that remained alive until this age) using the same task (Fig. 3K). The NORT memory test showed that at the age of 17 months (3 months after the first memory test and virus injection), overexpression of M7CK rescued the memory deficits in *5XFAD* mice that were observed at the age of 14 months (Fig. 3L). The total distance traveled during habituation and total number of explorations did not differ for any mice before and after M7CK overexpression (fig. S4, G and H). Thus, M7CK overexpression in the hippocampus prevented and reversed learning and memory deficits in *5XFAD* mice.

Overexpression of M7CK rescues synaptic density and reduces Aβ plaques

To explore whether M7CK overexpression could protect excitatory synaptic density in *5XFAD* mice, the brains of the mice used in the behavioral analysis above were collected for histological analysis at 15 months of age. The data showed that the synaptophysin and PSD-95 puncta density in the CA1 stratum radiatum was significantly reduced in *5XFAD* mice compared with WT mice; however, the puncta density was rescued by M7CK overexpression in the hippocampi of *5XFAD* mice (Fig. 4A). Similar results were found in *APP/PS1* mice: M7CK overexpression in the hippocampus rescued synaptophysin puncta density in the CA1 stratum radiatum at 19 months of age (fig. S5A). Regarding inhibitory synapses in *5XFAD* mice, we found that vesicular γ-aminobutyric acid (GABA) transporter (VGAT) puncta density did not change in these mice compared to WT and that M7CK overexpression did not cause any changes in the puncta density (fig. S5B). The lack of changes in inhibitory synapses in *5XFAD* mice observed here is in line with previous studies [(*32*), but see also (*33*)].

We also examined whether M7CK overexpression could reduce Aβ plaques in the hippocampus. Quantitative analysis indicated that compared with control *5XFAD* mice, *5XFAD* mice overexpressing M7CK in the hippocampi had significantly reduced Aβ plaque deposition in the hippocampus (Fig. 4B). To further verify these observations, we injected AAV-EGFP or AAV-M7CK-EGFP bilaterally into the hippocampi of additional groups of *5XFAD* at the age of 5 months. One month later, hippocampal tissue was collected to measure the soluble and insoluble $A\beta_{1–42}$ and $A\beta_{1–40}$ levels by using enzyme-linked immunosorbent assay (ELISA). We found that the levels of soluble and insoluble $A\beta_{1–42}$ were significantly reduced in *5XFAD* mice overexpressing M7CK compared with *5XFAD* mice (Fig. 4C). Only the level of the insoluble form of $A\beta_{1–40}$ was significantly reduced by M7CK overexpression (Fig. 4C). We also checked whether M7CK could reduce Aβ levels in vitro. We collected samples from hippocampal neuronal cultures exposed to high extracellular concentrations of Aβ (for 48 hours, with or without M7CK overexpression). We found that M7CK overexpression resulted in a significant reduction in $A\beta_{1–42}$ concentrations in neuronal cell lysates (Fig. 4D). Therefore, M7CK overexpression reduced Aβ plaques and restored synaptic density. M7CK appeared to reduce Aβ levels in vitro and in vivo.

M7CK promotes Aβ degradation by interacting with and activating MMP14

The rescue of memory functions and synapse density induced by M7CK overexpression was expected considering our previous studies in TRPM7 knockout mice showing that the kinase domain is a major regulator of synaptic and cognitive functions (*16*). However, we did not anticipate that M7CK overexpression could reduce Aβ plaques and Aβ levels. To explore how M7CK can decrease Aβ concentrations, we prepared new groups of mice: WT mice, WT mice overexpressing M7CK, *5XFAD* mice, and *5XFAD* mice overexpressing M7CK. The mice received bilateral injections of AAV-EGFP or AAV-M7CK-EGFP at 5 months of age. One month later, the mice were sacrificed, and hippocampal tissue was collected. We first checked whether M7CK might affect Aβ production. We quantified the expression of β-amyloid precursor protein (APP), β-secretase 1 (BACE1), presenilin-1 (PSEN1), and the β-cleaved carboxyl fragment of APP (βCTF) and found that their expression levels did not differ between *5XFAD* and M7CK-overexpressing *5XFAD* mice (Fig. 5A). Thus, we concluded that M7CK overexpression did not reduce the Aβ level by reducing its production. Autophagy is one of the major mechanisms involved in regulating Aβ clearance (*34*). Activation of TRPM7 reduces Aβ levels in neuroblastoma cells, probably by autophagy-dependent mechanisms (*21*). We checked the expression and phosphorylation levels of mammalian target of rapamycin (mTOR) p70 ribosomal S6 kinase (S6K), two major regulators of autophagy (*35*), and found no differences between *5XFAD* and *5XFAD* mice overexpressing M7CK (fig. S6, A to C). Thus, we concluded that M7CK overexpression did not reduce Aβ levels in *5XFAD* mice by promoting autophagy.

Then, we assessed the expression and phosphorylation of Aβ-degrading enzymes (*9*). Quantitative Western blot analysis revealed that the expression levels of IDE, NEP, ACE, and MMP14 did not differ between control *5XFAD* mice and M7CK-overexpressing *5XFAD* mice (Fig. 5B). Unlike the levels of the other proteins, MMP14 activity could be increased by phosphorylation (*36*, *37*). Thus, we quantified the phosphorylation level of MMP14 and found that it was increased mainly in *5XFAD* mice overexpressing M7CK (Fig. 5B). These data suggest that M7CK might promote Aβ clearance by overactivating MMP14. Therefore, it can be speculated that MMP14 might be an interaction partner and a possible phosphorylation target of M7CK. To examine this possibility, we performed coimmunoprecipitation experiments. Pulldown experiments in human embryonic kidney (HEK) cells using either a commercially available MMP14 antibody (Fig. 6A) or a customized M7CK antibody (Fig. 6B; for a validation experiment, see fig. S7A) revealed that these proteins were coimmunoprecipitated. Two other proteins related to MMP14 that might also contribute to Aβ degradation, namely, MMP9 (*38*) and MMP2 (*39*), were not detected in the protein complex that was pulled down, suggesting that M7CK specifically interacted with MMP14 (Fig. 6B). To check whether MMP14 could be phosphorylated by M7CK, we conducted an enzymatic activity assay by using purified proteins. Two negative controls, one in which M7CK was omitted and one in which the kinase was included but no substrate was added, were used (the latter was used as a control for comparisons). Myelin basic protein (MBP), a well-known substrate commonly used to assess M7CK activity (*40*), was used as a positive control for M7CK kinase activity. The results showed that enzymatic activity in the

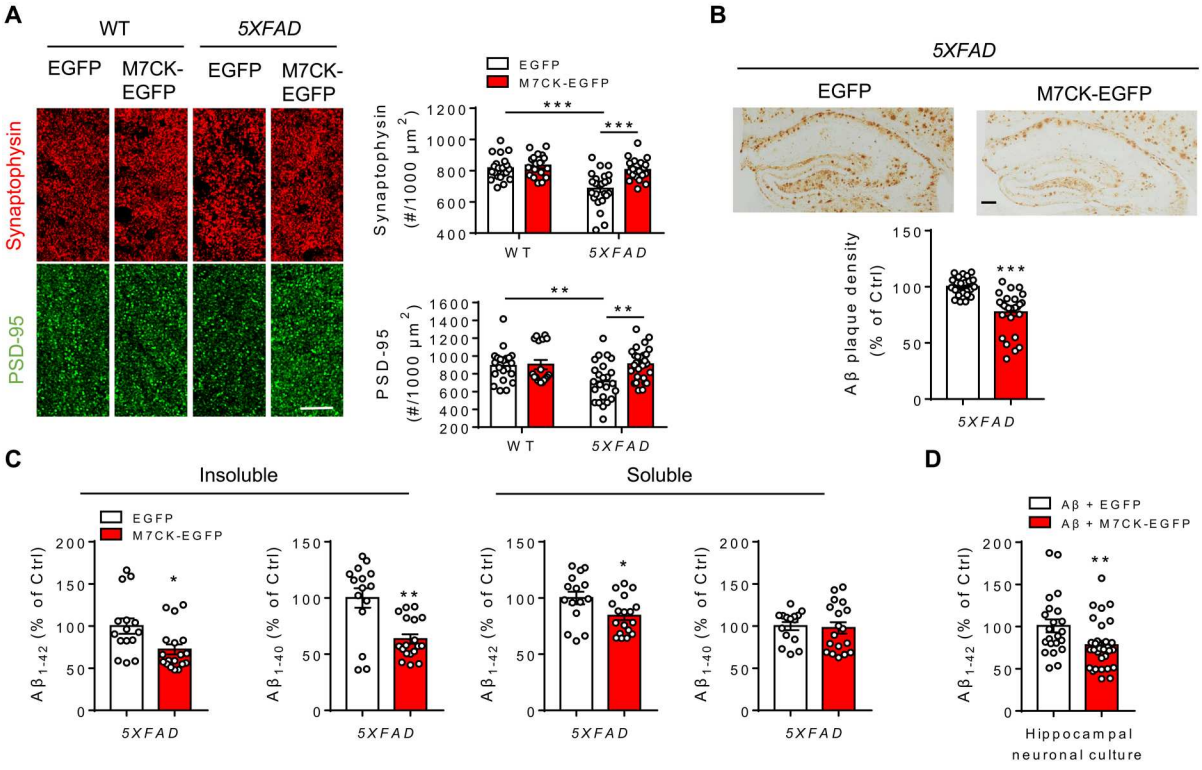

Fig. 4. Overexpression of M7CK in the hippocampus of *5XFAD* mice rescues AD-like pathologies. (**A**) Representative images (left) and quantitative analysis (right) of synaptophysin/PSD-95 puncta density in the stratum radiatum of CA1 area of WT and *5XFAD* mice at the age of 15 months with bilateral hippocampal injections of AAV-EGFP or AAV-M7CK-EGFP. *N* = at least 18 brain sections from six mice per group, analyzed by two-way ANOVA followed by Bonferroni's post hoc test. Scale bar, 10 μm. (**B**) Representative images (top) and quantitative analysis (bottom) of hippocampal amyloid plaques in *5XFAD* + EGFP (*n* = 24 brain sections from eight mice) and *5XFAD* + M7CK-EGFP mice (*n* = 27 brain sections from nine mice), analyzed by Mann-Whitney test. Scale bar, 200 μm. (**C**) Quantitative analysis of insoluble (left) and soluble (right) $A\beta_{1-42}$ and $A\beta_{1-40}$ using ELISA in hippocampal lysates from 6-month-old *5XFAD* mice with bilateral hippocampal injections of AAV-EGFP (*n* = 15 mice) or AAV-M7CK-EGFP (*n* = 18 mice), analyzed by Mann-Whitney test (insoluble/left) or unpaired *t* test (soluble/right). (**D**) Quantitative analysis of $A\beta_{1-42}$ in homogenates of Aβ-treated neuronal cultures after AAV-EGFP or AAV-M7CK-EGFP transduction. *N* = 22 and 30 homogenates, respectively, analyzed by Mann-Whitney test. For each mouse, three brain sections were used for immunohistochemistry quantitative analysis. **P* < 0.05, ***P* < 0.01, and ****P* < 0.001 by the test specified, with further details in tables S3 and S4.

reactions containing M7CK + MMP14 was significantly higher than that in reactions containing M7CK without substrate and was almost similar to that in the positive control reaction (M7CK + MBP; Fig. 6C). However, enzymatic activity in reactions containing MMP2 as a substrate (M7CK + MMP2) was similar to that in the control reaction. Thus, M7CK directly interacted with and phosphorylated MMP14.

To determine whether the interaction of M7CK with MMP14 and M7CK-mediated activation of MMP14 can promote Aβ degradation, we performed a series of in vitro protein degradation assays. Four groups of reactions were prepared. Aβ was incubated alone (control) or with the purified M7CK protein, MMP14, or M7CK + MMP14 for 10 hours in zymogen buffer containing adenosine 5′-triphosphate (ATP), which included all essential components for the phosphorylation reaction at proper concentrations. After incubation, protein was collected from each reaction, and the level of remaining Aβ was measured by using Western blotting. The level of Aβ was used as an indicator of the clearance efficiency (lower Aβ levels indicated faster clearance). We found that the Aβ level was reduced by ~30% in the reaction containing MMP14 compared with the control Aβ reaction (Fig. 6D). The Aβ level was reduced by ~65% in the reaction containing M7CK and MMP14 together, but not the reaction containing M7CK alone, compared with the control Aβ reaction (Fig. 6D). These data suggest that M7CK increases MMP14 activity, promoting Aβ degradation.

To determine whether MMP14 mediates the protective effect of M7CK against Aβ toxicity, we generated two variants of small hairpin RNA (shRNA) sequences (referred to as #1-$MMP14_{shRNA}$ and #2-$MMP14_{shRNA}$) to knock down MMP14 in neuronal cultures and scrambled control shRNA (referred to as $Ctrl_{SCR}$). We confirmed that these $MMP14_{shRNA}$ effectively reduced MMP14 protein expression by ~75 and ~45%, respectively, without affecting the expression of MMP2 or MMP9 (fig. S7B).

In line with data above (Fig. 2), overexpression of M7CK in hippocampal neuronal cultures prevented the high Aβ concentration–induced reduction in the density of synaptophysin puncta, but this protective effect of M7CK was completely abolished when MMP14 was suppressed (Fig. 6E). It is worth noting that we observed reductions in synapse density after suppression of MMP14 expression in control cultures ($MMP14_{shRNA}$ without Aβ; Fig. 6E). This is in line with previous studies showing that MMP14 is a regulator of synaptic density and functions (*41*). Therefore, it is unclear whether the blocking of M7CK protective effects was due to loss of synapses because of MMP14 suppression or due to loss of M7CK-MMP14

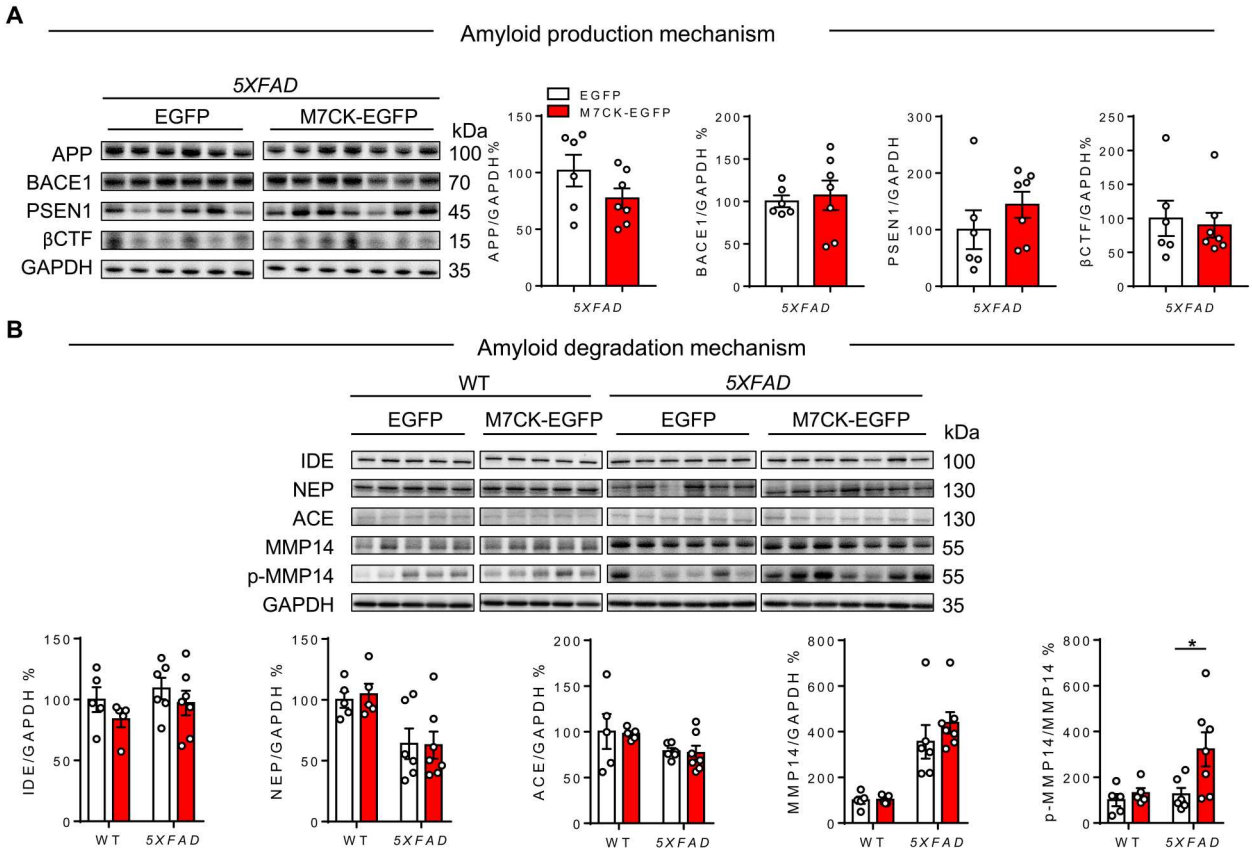

Fig. 5. Overexpression of M7CK increases the activity of the Aβ-degrading protein MMP14 without affecting Aβ production–related proteins. (**A**) Western blots (left) and quantitative analysis (right) of APP, BACE1, PSEN1, and βCTF proteins in the hippocampus of *5XFAD* mice at the age of 6 months with bilateral hippocampal injections of AAV-EGFP or AAV-M7CK-EGFP. The density of each band was first normalized to the corresponding GAPDH band co-detected on the same membrane, and then data were calculated as a percentage of average of the control group (*5XFAD* + EGFP). *N* = at least 6 mice per group, analyzed by (APP) unpaired *t* test, (BACE1) unpaired *t* test with Welch's correction, (PSEN1) unpaired *t* test, or (βCTF) Mann-Whitney test. (**B**) As described in (A) but of IDE, NEP, ACE, and MMP14 protein expression and MMP14 protein activation level (p-MMP14/MMP14). Data were calculated as a percentage of average of control group (WT + EGFP) from at least five mice per group, analyzed by two-way ANOVA followed by Bonferroni's post hoc test; *$P < 0.05$. Detailed information on sample sizes and statistical analyses are in tables S3 and S4. Full-length Western blots are provided in data file S1.

impact on Aβ toxicity. To further address the role of each protein and their interaction on AD-like pathology, we prepared hippocampal neuronal cultures from *5XFAD* mice and used Aβ level in culture medium (instead of synapse density) as a readout for MMP14 or M7CK suppression. We found that MMP14 knockdown increased Aβ abundance by ~21%. Knockdown of TRPM7 increased Aβ by ~43%. Overexpression of M7CK failed to reduce Aβ in the absence of MMP14 expression (Fig. 6F). Therefore, the TRPM7 kinase domain might interact with and activate the Aβ-degrading enzyme MMP14, resulting in higher Aβ clearance, which could lead to the observed reduction in Aβ plaques, protection of synaptic density, and preservation of memory functions in *5XFAD* mice.

DISCUSSION

Here, we found that TRPM7 expression was decreased in the hippocampi of patients with AD and mouse models of AD. The kinase domain, but not the ion channel part, of TRPM7 protected synapses from Aβ toxicity in vitro. Furthermore, it was effective in reducing Aβ plaques, protecting synaptic density, and preventing memory deficits in *5XFAD* mice. Mechanistically, we found that M7CK reduced soluble and insoluble Aβ levels by promoting Aβ degradation without affecting APP processing and/or autophagy. The results suggest that M7CK interacts with and activates the Aβ-degrading enzyme MMP14 to promote Aβ degradation and hence counteracts AD-like pathology (Fig. 6G).

Studies implicate TRPM7 in mediating pathologies of neurodegenerative diseases (*17*). After certain pathological triggers, overactivation of TRPM7 results in neurotoxic increases in intracellular calcium concentrations, resulting in neuronal death (*42*, *43*), whereas suppression of TRPM7 prevents neuronal death and cognitive deficits (*44*). Down-regulation of TRPM7 was found to exert protective effects in an in vitro model of Parkinson's disease (*45*). TRPM7 participates in Fas-induced cell apoptosis (*30*). The product of the *Fas* gene modulates apoptosis and neuronal loss during AD pathology (*46*). A previous study identified TRPM7 as a target of mixed lineage kinase domain–like protein (MLKL) in mediating cytotoxic calcium influx during necroptosis (*47*). MLKL-mediated necroptosis mechanisms are activated in the AD brain (*48*). The

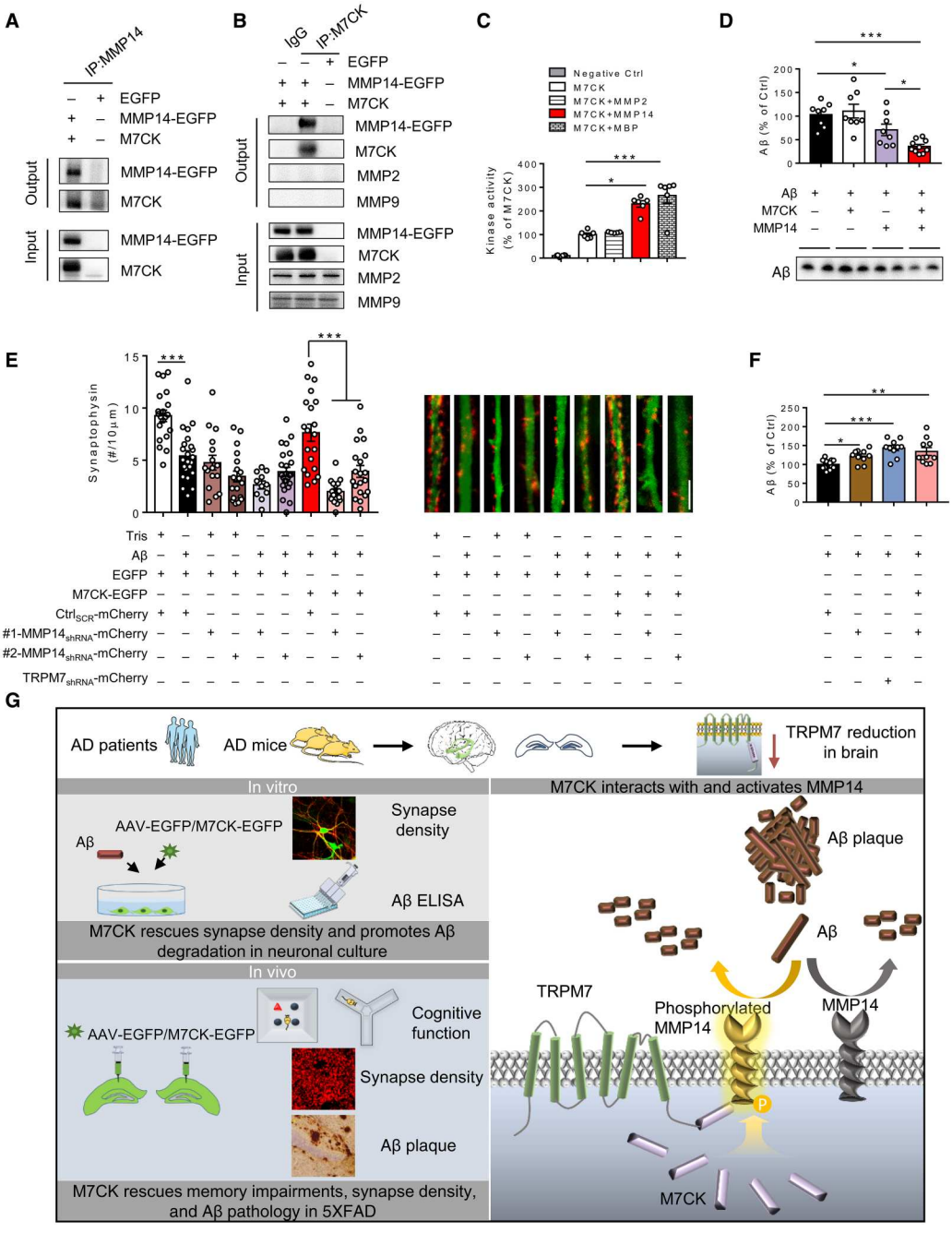

Fig. 6. M7CK interacts with and phosphorylates MMP14 to promote Aβ degradation. (**A** and **B**) Coimmunoprecipitation of M7CK and MMP14 from HEK 293T cells using antibody to MMP14 (A) or to M7CK (B). Blots are representative of two independent experiments. (**C**) Kinase enzymatic activity assay of M7CK using MMP14 or MMP2 as a substrate in cell-free in vitro reactions. MBP was used as a positive control. Negative controls (without substrate or without M7CK) are presented. Enzymatic activity was calculated as a percentage of average control, from at least five reactions per group, analyzed by one-way ANOVA Kruskal-Wallis test. (**D**) Quantitative analysis (top) and representative Western blots (bottom) of the remaining Aβ as an indicator of Aβ degradation after being incubated with cell-free in vitro reactions containing Aβ only, Aβ + M7CK, Aβ + MMP14, or Aβ + MMP14 + M7CK proteins. Data are presented as a percentage of the average control (Aβ only), from at least eight reactions per group, analyzed by one-way ANOVA followed by Bonferroni's post hoc test. (**E**) Quantitative analysis (left) and representative fluorescent images (right) of synaptophysin puncta density in hippocampal neuronal cultures incubated with tris buffer or Aβ and transduced with AAV-EGFP or AAV-M7CK-EGFP accompanied by AAV-Ctrl$_{SCR}$-mCherry, AAV-#1MMP14$_{shRNA}$-mCherry, or AAV-#2MMP14$_{shRNA}$-mCherry. EGFP, mCherry, and synaptophysin signals were imaged through 488, 594, and 647 channels, respectively. *N* = at least 11 neurons from three independent neuronal cultures per group, analyzed by one-way ANOVA followed by Bonferroni's post hoc test. The mCherry signal of AAV-Ctrl$_{SCR}$ or AAV-MMP14$_{shRNA}$ was omitted, and green color (EGFP) was used to label dendrite. Scale bar, 5 μm. (**F**) Quantitative analysis of Aβ$_{1–42}$ in medium from *5XFAD* neuronal cultures transduced with AAV-Ctrl$_{SCR}$-mCherry, or AAV-#1MMP14$_{shRNA}$-mCherry, or AAV-TRPM7$_{shRNA}$-mCherry, or AAV-M7CK-EGFP and AAV-#1MMP14$_{shRNA}$-mCherry. *N* = at least 10 neuronal cultures per group, analyzed by one-way ANOVA followed by Bonferroni's post hoc test. (**G**) Graphic depiction summarizing the study and illustrating the mechanism uncovered. In (A) to (F), $^{*}P < 0.05$ and $^{***}P < 0.001$ by the test specified, with detailed sample size and statistical analysis information in tables S3 and S4, and full-length Western blots in data file S1.

kinase domain of TRPM7 is an important activator of annexin 1 (*49*), which is overactivated in the AD brain (*50*). Overexpression of CD82 in HEK cells promotes cleavage of the TRPM7 kinase domain, leading to increases in Numb phosphorylation, which promotes Aβ production and toxicity (*51*). Thus, TRPM7 overactivation/overexpression is proposed as one of the pathological changes mediating neuronal death during neurodegenerative disorders, and its suppression can be considered as a therapeutic strategy to treat such disorders (*17*).

On the other hand, studies provide direct and indirect links between TRPM7 hypoactivation/down-regulation and AD pathology, supporting the notion that overexpression/overactivation of TRPM7 might help counteract such pathological changes. For instance, a mutation in TRPM7 that reduces its channel functions has been linked to a neurodegenerative disorder characterized by

motor and cognitive dysfunctions (*18*). In vitro studies show that activation of TRPM7 by phosphatidylinositol 4,5-bisphosphate decreases Aβ levels in cell lines with familial AD–associated mutations (*19*, *20*). In neuroblastoma cells, activation of TRPM7 channels increases basal autophagy and reduces Aβ levels (*21*). In vitro and in vivo studies show that deletion of TRPM7 and/or its kinase domain or suppression of its expression results in synaptic and cognitive dysfunctions (*16*, *22*, *23*). Synapse loss and memory deficits are among the major hallmarks of AD pathology (*1*). TRPM7 and/or its kinase domain are known to be a part of the complex regulating the cytoskeleton, which is necessary for cell migration, protrusion, adhesion, and survival (*52*, *53*). Abnormalities in cytoskeleton dynamics have been reported in AD cases (*54*). In this study, we found that TRPM7 expression was reduced in the AD brain and the brain of two mouse models of AD. Overexpression of the kinase domain was sufficient to counteract Aβ toxicity in cultured neurons and AD-like pathology in vivo by promoting Aβ degradation. The differences in the reported roles of TRPM7 in the pathologies of neurodegenerative disorders could stem from differences in the models used (in vitro versus in vivo models, cell lines versus primary neuronal cultures) and/or the pathological triggers used to study neurodegenerative disorders.

TRPM7 is known as an important regulator of MMP activity during cancer cell metastasis (*55*, *56*). MMP14 is active by default, but its activity can be further increased by phosphorylation (*36*, *37*). In astrocytes, an increase in MMP14 expression promotes Aβ degradation, resulting in a reduction in its accumulation (*11*). Our Aβ metabolism assay shows that MMP14 can degrade Aβ on its own. Furthermore, increasing MMP14 activity by M7CK-mediated phosphorylation further increased Aβ degradation. However, we found that MMP14 expression was increased in *5XFAD* mice. Thus, although it may promote Aβ degradation, overexpression of MMP14 is not sufficient to rescue AD-like pathologies because these mice still exhibit synaptic and cognitive dysfunctions. Meanwhile, M7CK activated MMP14 and rescued AD-like pathologies. M7CK alone without MMP14 failed to rescue synapse density and/or reduce Aβ concentration. Therefore, our results suggest that M7CK may be one of the upstream kinases that can induce sufficient activation (not overexpression) of MMP14 in the brains of *5XFAD* mice to counteract AD-like pathologies.

Studies in APP-expressing HEK cells show that MMP14 might increase Aβ and βCTF production by promoting APP processing via endosome-dependent mechanisms (*57*). In *5XFAD* mice, we found that M7CK overexpression increased MMP14 activity, but we did not detect any changes in APP or βCTF levels, although MMP14 was up-regulated, suggesting that increases in MMP14 expression and activity have no amyloidogenic effects, at least in *5XFAD* mice. In contrast, our Aβ degradation assay suggested that M7CK and MMP14 together can promote Aβ degradation. However, both M7CK (*16*) and MMP14 (*41*) were shown to be important for synaptic density and synaptic functions. Thus, we cannot exclude the possibility that, in addition to promoting Aβ degradation, M7CK and MMP14 may affect other signaling pathways regulating synaptic density/function to contribute to rescuing memory functions in *5XFAD* mice. In addition, Aβ can be cleared by the autophagy-lysosome system (*34*). Previous studies have shown that TRPM7 reduces Aβ levels by activating autophagy in the SH-SY5Y cell line (*21*). We did not detect an increase in the activation of autophagy initiation factors after overexpressing M7CK in the brain. It is possible that the effects on autophagy are model dependent (cell lines versus brain tissue from *5XFAD* mice, mitotic astrocytes or neuroblastoma cells versus postmitotic glutamatergic neuronal cells) or that they depend on the ion channel portion of TRPM7 in mitotic cells. Nevertheless, the role of TRPM7 in Aβ degradation and clearance is becoming increasingly evident; hence, future studies should further elucidate the mechanisms mediating the effects of TRPM7 and its kinase domain on Aβ levels.

In conclusion, this study provides mechanistic insights into the role of TRPM7 in amyloid-associated neurodegenerative disorders, particularly AD. Our results show that AD pathology is associated with a reduction in TRPM7 expression and that maintaining normal expression of its kinase domain is sufficient to reduce Aβ accumulation, protect synaptic density, and prevent or reverse memory deficits.

MATERIALS AND METHODS

Experimental animals

5XFAD male mice (B6SJL-Tg [APP-SwFlLon, PS1*M146L*L286V] 6799Vas/J, JAX stock number: 034840) were crossed with WT female mice (C57BL/6). Offspring were kept as hemizygous and genotyped according to protocol from the Jackson Laboratory. *APP/PS1* male mice (B6.Cg-Tg [APPswePSEN1dE9], JAX stock number: 034832) were purchased from Model Animal Research Center of Nanjing University (China). Newborn WT mice for primary hippocampal neuronal culture and WT mice for breeding *5XFAD* mice were purchased from Jie Si Jie Laboratory Animal Company (China). Mice were group-housed (three or four mice per cage) under a controlled environment of 21°C ± 1, humidity 50 ± 10%, and a 12-hour/12-hour inverted light-dark cycle in Fudan University's laboratory animal center. All experiments involving animals were approved by Fudan University committees on animal care and use (license number: SYXK-2020-0032). All mice included in behavior and biochemical analysis were male mice unless mentioned otherwise.

AD patient brain samples

Human brain tissues were supplied by National Health and Disease Human Brain Tissue Resource Center (China Brain Bank, Zhejiang University School of Medicine). The ethical code and detailed information about patients with AD and healthy controls are provided in table S1. Tissue samples were from hippocampi of six patients with AD and five healthy controls. Braak's criterion evaluates the degree of tau pathology. Braak stages I/II, III/IV, and V/VI represent the spread of neurofibrillary tangles in entorhinal, limbic, and neocortical regions, respectively (*58*). The Consortium to Establish a Registry for Alzheimer's Disease (CERAD) criterion evaluates the density of amyloid plaques, and higher scores represent larger amyloid burdens (*59*). Experiments were conducted in accordance with China Brain Bank institutional guidelines and the institutional review board (Ethics Committee) of Shanghai Medical College guidelines (20110307-085, 20120302-099).

Primary hippocampal neuronal cultures and Aβ treatment

Hippocampi of WT postnatal day 1 to 3 mice pups were carefully dissected in ice-cold dissection medium (Sigma-Aldrich, #M0518). Then, hippocampi were cut into pieces and digested using trypsin (Sigma-Aldrich, #T1005) with deoxyribonuclease (Sigma-Aldrich,

#D5025) for 5 min at 37°C, followed by cell dissociation chemically and mechanically. Last, cell suspension was seeded on coverslips (14-mm diameter and 0.17-mm thickness) and cultured for up to 14 days in vitro (DIV) before use. Cultures were maintained at 37°C in a humidified 5% CO_2 atmosphere. Sister cultures from the same batch were always used and treated on the same day (divided into control and/or experimental groups). The experimental results from hippocampal neuronal cultures were obtained from at least three independent cultures per group. At 7 DIV, cultures were transduced with AAV-CAG-EGFP, AAV-CAG-M7CK-EGFP, AAV-CAG-M7CK-K1646R-EGFP, AAV-CAG-GPI-EGFP-GPI, AAV-CAG-GPI-M7CK-EGFP-GPI, LV-EGFP, or LV-TRPM7ΔK-EGFP virus. To knock down MMP14, neuronal cultures were transduced with AAV-CAG-scrambled-shRNA-mCherry or AAV-CAG-MMP14-shRNA-mCherry virus accompanied by AAV-CAG-EGFP or AAV-CAG-M7CK-EGFP virus at 7 DIV. $A\beta_{1–42}$ peptide (Tocris, #1428) was dissolved in 50 mM tris (pH 7.4) buffer at a concentration of 1 μg/μl (200 μM) and stored as aliquots at −20°C until use. At 12 DIV, 2.5 μl of Aβ peptide aliquots was added in neuron culture medium to a final concentration of 500 nM, and the same volume of 50 mM tris buffer was added into the culture medium of the control group. At 14 DIV, immunostaining of neuronal cultures was conducted. To overexpress full-length TRPM7/P1040R/K1646R, neuronal cultures were transfected with 1 μg of plasmid per 1 ml of cultural medium by Lipofectamine 2000 (Thermo Fisher Scientific, #11668027) at 4 DIV and immunostained at 14 DIV. Aβ treatment was the same as above. Hippocampi of *5XFAD* postnatal day 1 to 3 mice pups were cultured using the same protocol as above, transduced with AAV virus at 7 DIV, and collected at 14 DIV. To knock down TRPM7, neuronal cultures were transduced with AAV-CAG-scrambled-shRNA-mCherry or AAV-CAG-TRPM7-shRNA- mCherry virus. AAV virus was added at a volume of 1 μl per 1 ml of culture medium (AAV virus titer is mentioned at AAV virus production part), and LV-EGFP or LV-TRPM7ΔK-EGFP virus was added at a volume of 1 or 4 μl per 1 ml of culture medium (respectively: LV-EGFP virus titer: 5×10^8 genomes/ml and LV-TRPM7ΔK-EGFP virus titer: 2×10^7 genomes/ml).

Viral vectors, plasmids, and clones

The TRPM7 (GenBank ID: #NM_001164325.1) α-kinase domain (M7CK, amino acids 1299 to 1863 of TRPM7 sequence), which has been shown to be functional before (*15*, *16*), was amplified from mouse hippocampal complementary DNA (cDNA) and cloned into AAV-CAG-EGFP plasmid backbone (Addgene, plasmid no. 37825). Mutant kinase (M7CK-K1646R) sequence was synthesized (Obio Technology) and cloned into the same AAV-CAG-EGFP plasmid. Mouse truncated TRPM7 ion channel sequence (TRPM7ΔK, amino acids 1 to 1510 of TRPM7 sequence), which was proven to be functional (*30*), was synthesized, cloned into Lenti-CMV-EGFP-3Flag vector, and packaged into lentivirus by Obio Technology. WT full-length TRPM7 (amino acids 1 to 1862) was synthesized and cloned into pEGFP-N1 plasmid (Obio Technology). Full-length TRPM7 with inactive channel mutation P1040R (*31*) or with inactive kinase mutation K1646R (*29*) were constructed. To generate cell membrane–anchored M7CK, an AAV-CAG-GPI-M7CK-EGFP-GPI vector was generated with two synthesized GPI sequences at both sides of M7CK-EGFP (N-anchor amino acids: MGIQGGSVLFGLLLVLAVFCHSGHS, C-anchor amino acids: MGIQGGSVLFGLLLVLAVFCHSGHS). For cloning MMP14, the coding sequence (GenBank ID: #NM_008608.4) was amplified from mouse hippocampal cDNA and cloned into the pEGFP-N1 plasmid.

Generation of MMP14 shRNA and TRPM7 shRNA

MMP14 shRNA and control scrambled shRNA were synthesized and constructed to AAV-CAG-mCherry plasmid (GeneChem). #1-MMP14 shRNA sequence binding to the mouse MMP14 (1026-1046 of the coding sequence, GenBank ID: #NM_008608.4) was 5′-ACCGGGCGGGTGAGGAATAACCAAGTCTCGAGACT TGGTTATTCCTCACCCGCTTTT-3′. #2-MMP14 shRNA sequence binding to the mouse MMP14 (788-808 of the coding sequence) was 5′-ACCGGGGATGGACACAGAGAACTTCGCTC GAGCGAAGTTCTCTGTGTCCATCCTTTTT-3′. The scrambled shRNA sequence was 5′-CGCTGAGTACTTCGAAATGTC-3′. TRPM7 shRNA and control scrambled shRNA were as previously reported (*16*). The TRPM7 shRNA sequence binding to the rat TRPM7 (5153-5172 of the coding sequence) was 5′-AATGCATG ACTGGGGAATTTCAAGAGAATTCCCCAGTCATGCATT-3′. The negative control scramble shRNA sequence was 5′-ATAAGA ACAGCGGCTATATTCAAGAGATATAGCCGCTGTTCTTAT-3′.

AAV production

HEK 293T cells were thawed and cultured in Dulbecco's modified Eagle medium (GIBCO, #11995-065) containing 10% fetal bovine serum (GIBCO, #10099141) and 1% antibiotics (penicillin/streptomycin, 100 U/ml; GIBCO, #15140-122) incubated in a humidified chamber containing 5% CO_2 at 37°C. After being digested by trypsin (GIBCO, #25200-056), cells were passaged to 15-cm culture plates. Once covering 70 to 80% of the surface of the culture plate, cells were cotransfected with AAV plasmid and the AAV virus packaging helper plasmids by using VigoFect transfection reagent (Vigorous Biotechnology, #T001). The transfected cells were lysed completely by digestion enzymes (Sigma-Aldrich, #E1014-25KU). AAV virus particles were purified from cell lysates by heparin columns (HiTrap Heparin HP, Cytiva, #17040601), washed by gradient low-concentration salt solutions [100, 150, 200, and 300 mM NaCl in 20 mM tris (pH 8.0)], eluted by gradient high-concentration salt solutions [400, 450, and 500 mM NaCl in 20 mM tris (pH 8.0)], and condensed by centrifugation at 2000*g*, 4°C using centrifugal filters tubes (Amicon Ultra-4, Millipore, #UFC810096) until the liquid (containing virus particles) inside the filter was less than 200 μl. The virus titer was assessed by real-time quantitative polymerase chain reaction (PCR) using TaqMan Universal Master Mix (Applied Biosystems, #UNG4440038) at LightCycler M480 machine (Roche, Switzerland). The titered AAV virus was diluted to nearly 3×10^{12} to 5×10^{12} genomes/ml by phosphate-buffered saline (PBS). The virus efficiency was further detected through gradient transfection of HEK 293T cells and validated by microinjection into mice brain. Plasmids for AAV virus packaging are listed as follows: AAV-CAG-EGFP, AAV-CAG-M7CK-EGFP, AAV-CAG-GPI-EGFP-GPI, AAV-CAG-GPI-M7CK-EGFP-GPI, AAV-CAG-scrambled-shRNA-mCherry, and AAV-CAG-MMP14-shRNA-mCherry plasmids.

Virus injection

Mice were anesthetized under 2% isoflurane at the age of 5 months and fixed in a stereotaxic frame (RWD Instruments). The virus

injection coordinates for the hippocampus were mentioned as follows according to the parameters described in Paxinos and Franklin's "The Mouse Brain in Stereotaxic Coordinates" (third edition): anterioposterior (AP) = −2.06 mm, mediolateral (ML) = ±1.4 mm, dorsoventral (DV) for CA1 = 1.4 mm and for dentate gyrus = 2.0 mm. Coordinates for CA3 AP = −2.06 mm were ML = ±2.25 mm and DV = 2.1 mm. Bilateral injections of 300 nl of virus (AAV-CAG-EGFP, AAV-CAG-M7CK-EGFP) were infused in each site at a rate of 1 nl/s through glass capillary driven by Nanoject III pump (Drummond), for a total of 1.8 μl of virus per mouse. The needles were left in place for more than 10 min before they were removed. After suturing, the mice were kept in a warm chamber to recover from anesthesia and then returned to their homecages. After 1 month, behavioral assays and/or biochemical analyses were performed. For the reversal experiments, eight male and eight female *5XFAD* mice were injected with the same amount of virus (AAV-CAG-EGFP and AAV-CAG-M7CK-EGFP) into the hippocampus at the age of 14 months as described above, and the aging mice were evaluated behaviorally at the age of 17 months.

Western blotting

Total protein was extracted from freshly dissected hippocampal tissues using radioimmunoprecipitation assay (RIPA) buffer (Beyotime, #P0013B) with protease and phosphatase inhibitor cocktail (Roche, nos. 04906837001 and 04693159001). Total protein concentration was determined by bicinchoninic acid (BCA) kit (Thermo Fisher Scientific, #23225). APP, βCTF, and Aβ protein bands were separated by Biofuraw precast 4 to 12% bis-tris gel (Tanon, #180-8018) and detected by Aβ6E10 antibody (1:2000; BioLegend, #803001). Other protein bands were separated by 10 to 15% SDS–polyacrylamide gel electrophoresis (SDS-PAGE) gel. The separated bands were transferred onto 0.45-μm polyvinylidene difluoride membranes (Millipore, #IPVH00010). After blocking (5% skim milk and 0.1% Tween in PBS), membranes were incubated with primary antibody overnight at 4°C. After washing, membranes were incubated with anti-rabbit (1:5000; SAB, #L3012) or anti-mouse (1:5000; Cell Signaling Technology, #7076S) horseradish peroxidase (HRP)–conjugated antibody for 1.5 hours at room temperature. Then, membranes were visualized by incubating them with enhanced chemiluminescence solution (Tanon, #180-5001) and imaged by Tanon 5200 multi-imaging system. In addition, images were analyzed by Gel Pro Analyzer software (Media Cybernetics). The integrated optical density (IOD) of targeted protein bands was measured and normalized to the IOD of glyceraldehyde-3-phosphate dehydrogenase (GAPDH) (the housekeeper protein). Primary antibodies used in Western blotting were listed as follows: GAPDH (1:10,000; Proteintech, #10494-1-AP), NEP (1:200; Santa Cruz Biotechnology, #sc46656), IDE (1:1000; Santa Cruz Biotechnology, #sc393887), ACE (1:200; Santa Cruz Biotechnology, #sc23908), MMP14 (1:2000; Abcam, #AB51074), phosphoserine/threonine (for detecting p-MMP14, 1:1000; BD Biosciences, #612548), MMP2 (1:2500; Millipore, #MAB3308), MMP9 (1:1000; Millipore, #AB19016), Aβ 6E10 (1:2000; BioLegend, #803001), BACE1 (1:1000; Cell Signaling Technology, #D10E5), PSEN1 (1:500; Santa Cruz Biotechnology, #sc365450), mTOR (1:1000; Novus, #BP1-19855), p-mTOR (1:1000; Novus, #BP1-19934), S6K (1:1000; Millipore, #04-391), and p-S6K (1:1000; Millipore, #04-392). Two TRPM7 antibodies were used in the current study; the first antibody is commercially available targeting the ion channel part (amino acid sequence 1146 to 1165 of human TRPM7 sequence, 1:750; Alomone, #ACC-047). Another antibody was customized and made for us to target the kinase domain of TRPM7 (M7CK, amino acid sequence 1300 to 1539 of mouse TRPM7, 1:500; Abclonal, customized). Validation of M7CK antibody is shown in fig. S7A.

Reverse transcription PCR

Total RNA of hippocampal tissues from human and *5XFAD* mice brain was extracted using TRIzol reagent (Ambion, #15596018) according to the manufacturer's instructions. One microgram of total RNA was converted into cDNA by using SuperScript II reverse transcriptase (Invitrogen, #18064-014). Primer sequence was designed using Primer-BLAST (National Center for Biotechnology Information) as follows: TRPM7 primer sequence for human and mouse: sense, 5′-GATGAAACGATGGCTATGAAA-3′ and antisense, 5′-ATATGGCAGGTGGAACTAAAA-3′; GAPDH primer sequence for human: sense, 5′-GGCTGCTTTTAACTCTGGTAAAG-3′ and antisense, 5′-CATTGATGACAAGCTTCCCG-3′; and GAPDH primer sequence for mouse: sense, 5′-AGAGTGTTTCCTCGTCCCGTA-3′ and antisense, 5′-TCGCTCCTGGAAGATGGTGAT-3′. PCR was performed using Premix Taq (Takara, #RR901) by adding the same amount of cDNA and primers. GAPDH was used as internal reference. After electrophoresis, the bands were visualized and imaged by Tanon 1600. In addition, images were analyzed by ImageJ. The IOD of targeted DNA bands was measured and normalized to that of corresponding GAPDH band.

Coimmunoprecipitation

HEK 293T cells were cultured as mentioned above (see the "AAV production" section). When covering 70 to 80% of the surface area of the cell culture plates (35-mm diameter, Thermo Fisher Scientific, #140675), HEK 293T cells were transfected with 4 μg of DNA carrying MMP14-EGFP by using Lipofectamine 2000 (Invitrogen, #52887). After 48 hours, cells were harvested and homogenized in RIPA buffer (Beyotime, #P0013C) containing protease and phosphatase inhibitors, kept on ice for 20 min, and centrifuged at 12,000 rpm for 30 min at 4°C. The supernatant was collected and used in the following steps. Coimmunoprecipitation of recombinant MMP14 and native cleaved kinase domain was performed according to the manufacturer's instructions of the Dynabeads Protein G Immunoprecipitation Kit (Invitrogen, #10007D). Two micrograms of MMP14 antibody (Abcam, #AB51047) or the customized M7CK antibody (ABclonal, targets the native kinase domain of TRPM7) were incubated in 200 μl of antibody binding buffer containing 1.5 mg of Dynabeads on a mild rotator (60 rpm) at room temperature for 30 min. Afterward, supernatant was removed on magnet (Thermo Fisher Scientific, #MR02). Then, 150 μl of samples containing antigen were mixed with the bead-antibody complex and incubated on rotator for 42 hours at 4°C. The bead-antibody-antigen complex was washed, transferred to a new tube, and eluted by elution buffer followed by denaturation at 99°C for 5 min. The supernatant was pipetted on magnet, loaded in 10% SDS-PAGE, and detected using Western blotting as described above.

Fluorescent immunostaining

For immunostaining in brain sections, anesthetized (as described above) mice were perfused transcardially with 0.9% saline followed by 4% paraformaldehyde (PFA). Brains were removed, postfixed in 4% PFA overnight, and dehydrated in gradient sucrose. Next, brains were embedded in optimal cutting temperature compound (Tissue Tech, #4583) and stored at −80°C. Frozen coronal sections (16 μm) were cut, mounted on slides, and left to dry for 5 to 6 hours. Afterward, the mounted brain sections were blocked in freshly prepared blocking solution (5% goat serum and 0.2% Triton X-100 in PBS) for 2 hours at room temperature followed by incubation with primary antibody diluted in blocking buffer overnight at 4°C. After washing with PBS, sections were incubated by CF-dye–conjugated secondary antibody with corresponding species for 2 hours at room temperature. Then, sections were incubated with 4′,6-diamidino-2-phenylindole (DAPI; 1:1000; Sigma-Aldrich, #D9542) for 10 min at room temperature. Last, sections were covered using appropriate amount of anti-quenching mounting solution (Sangon Biotech, E675005-0010). Only for CaMKII immunochemistry, floating sections were used and incubated with primary antibody overnight at room temperature, and then brain sections were mounted on slides at the final stage. For immunostaining in neuronal cell cultures, 14 DIV hippocampal neuron cultures were fixed using 4% PFA for 45 min. The following procedures were the same as immunostaining of brain sections. Primary antibodies were used as follows: TRPM7 targeting ion channel part (1:50; Alomone, #ACC-047), CaMKII (1:500; Abcam, #ab22609), GAD67 (1:200; R&D Systems, #AF2086), NeuN (1:500; Abcam, #ab177487), IBA1 (1:1000; Wako, #019-19741), GFAP (1:500; Millipore, #MAB360), GAD65/67 (1:500; Sigma-Aldrich, #G5163), synaptophysin (1:500: Synaptic Systems, #101011), PSD-95 (1:100; Cell Signaling Technology, #3450S) for brain section, PSD-95 (1:500; Synaptic Systems, #124003) for neuronal culture, and VGAT (1:200; Synaptic Systems, #131002). Secondary antibodies were used as follows: CF-488 goat anti-mouse conjugated secondary antibody (1:500; Biotium, #20010), CF-647 goat anti-mouse conjugated secondary antibody (1:500; Biotium, #20040), CF-488 goat anti-rabbit conjugated secondary antibody (1:500; Biotium, #20019), and CF-555 goat anti-rabbit conjugated secondary antibody (1:500; Biotium, #20033).

Synaptophysin and PSD-95 puncta analysis

In hippocampal neuron cultures, images of synaptophysin and PSD-95 puncta were taken by Olympus FluoView FV1000 confocal microscope using 60× numerical aperture (NA) 1.42 oil immersion lens with digital zoom 3 at a resolution of 1024 × 1024. Synaptophysin and PSD-95 puncta, which were located on single dendrite directly, were counted to measure density. Results are presented as puncta number per 10-μm dendrite per neuron. In brain sections, synaptophysin and PSD-95 images in stratum radiatum areas of the CA1 region were taken by Olympus FluoView FV1000 confocal microscope using 60× NA 1.42 oil immersion lens with digital zoom 3 at a resolution of 1024 × 1024. Serial *z* sections were taken at step size of 1 μm. Then, the three *z* sections with the strongest signals were stacked into a single image. Image-Pro Plus 6.0 (Media Cybernetics) was used to analyze puncta number, which was conducted according to previous research (*16*). HiGauss filters were used to enhance synaptophysin and PSD-95 signals. In addition, the same limited watershed split range was used in each image to split puncta. The total puncta number was calculated by the software. The puncta density was calculated and presented as total puncta number per 1000 μm^2. Three sections per mice were used for quantitative analysis.

TRPM7 density quantitative analysis

After TRPM7 immunostaining, serial *z* sections of each brain section were taken at a step size of 2 μm by using Olympus FluoView FV1000 confocal microscope equipped with 60× NA 1.42 oil immersion lens. Images were taken at a resolution of 1024 × 1024 within stratum radiatum areas of the CA1 region. Quantitative analysis was conducted as follows: Backgrounds from all images were reduced and set to a minimum equal level. Images were converted to grayscale and inverted contrast. Then, IOD of fluorescent signals was measured by Image-Pro Plus 6.0 software (Media Cybernetics). DAPI in stratum pyramidale of CA1 was counted by ImageJ software (NIH). For CaMKII/GAD and TRPM7 coimmunostaining, the IOD of TRPM7 was quantified inside cell bodies of CaMKII-/GAD-positive neurons. Both CaMKII/GAD and TRPM7 were imaged in the same experiment under similar microscopic conditions. Three sections per mice were used for quantitative analysis.

Imaging of AAV-CAG-M7CK-EGFP with CaMKII, GAD65/67, GFAP, or IBA1 staining

Brain sections overexpressing AAV-CAG-M7CK-EGFP were coimmunostained with CaMKII, GAD65/67, IBA1, and GFAP separately. All images were taken in the CA1 areas of the hippocampus by using Olympus FluoView FV1000 confocal microscope. CaMKII or GAD65/67 with M7CK-EGFP signals was imaged using 60× NA 1.42 oil immersion lens with digital zooms 1 and 3 at a resolution of 1024 × 1024. GFAP or IBA1 with M7CK-EGFP signals was imaged using 20× NA 0.75 lens with digital zoom 1 at a resolution of 1024 × 1024.

MMP14, M7CK, MMP2, and MBP clones, protein purification, and kinase enzymatic activity

MMP14 sequence (GenBank ID: #NM_008608.4), *M7CK* sequence (amino acids 1299 to 1863 of TRPM7 sequence), *MBP* sequence (GenBank ID: #NM_001025245.1), and *MMP2* sequence (GenBank ID: #NM_008610.3) were amplified from WT mouse hippocampus cDNA and cloned in pcDNA3.1$^+$ vector (Obio Technology). The constructed plasmid was transformed into DH5α competent cells (Weidi Biotechnology, #DL1001) and then spread on LB plate medium (10 g of tryptone, 5 g of yeast extract, 10 g of NaCl, and 15 g of agar powder into 1 liter of double-distilled water) containing $Kana^+$ (100 μg/ml; Sangon Biotech, #A100408) and cultured overnight at 37°C. Five or six single colonies were selected for sequencing (Sangon Biotech), and the correct one was used to amplify the protein overnight at 37°C for protein extraction. The amplified bacteria were centrifuged at 4200 rpm at 4°C, resuspended by lysis buffer [50 mM tris-HCl (pH 8.0), 100 mM NaCl, 10 mM $MgCl_2$, 1 mM EDTA, 10 mM β-mercaptoethanol, 20% glycerol, lysozyme (1 mg/μl), 8 M urea, and one pill of protease inhibitor], kept on ice for 30 min, and ultracentrifuged at 28,000 rpm for 30 min at 4°C (Beckman, Optima XPN-100 ultracentrifuge). The supernatant liquid was obtained and condensed at 4200 rpm at 4°C by Amicon Ultra 15 ML-30K protein isolation centrifugal filters (Millipore, #UFC9030) until the remaining liquid was less than 1 ml. The ultrafiltrates of each protein were collected and used for kinase activity

or in vitro Aβ degradation experiment. Ultrafiltrates from nontransformed bacteria were collected and used for negative controls.

Kinase activity was conducted by using a universal kinase activity assay kit (R&D Systems, #EA004). The purified MMP14, M7CK, and MMP2 proteins were diluted to 0.4 μg/μl by assay buffer and renatured at room temperature. As a positive control substrate for the kinase (*40*), MBP was also used at the same concentration. The proteins were added into reactions and incubated for 20 min at room temperature. Then, Malachite Green Reagent A and B were added to each reaction and incubated for 20 min at room temperature to generate color and stop enzymatic reaction. The optical density of each reaction was detected at 620 nm by MultiScan Go (Thermo Fisher Scientific). Reaction with adenosine 5′-diphosphate (ADP) instead of ATP was run as positive control to confirm that reactions occurred. Reactions without substrate or kinase (using ultrafiltrates from nontransformed bacteria) were run as negative controls. A blank was also run as a control. A calibration curve was constructed according to the user′s manual of the kit. All data were calculated as a percentage of the control (+M7CK but no substrate) group.

In vitro Aβ degradation experiment

M7CK and MMP14 proteins were extracted as described above (see MMP14 and M7CK protein extraction). $Aβ_{1–42}$ (2 μM; Tocris, #1428) was incubated with 80 nM M7CK only or MMP14 only or both MMP14 and M7CK proteins in zymogen buffer [50 mM tris-HCl, 200 mM NaCl, and 5 mM $CaCl_2$ (pH 7.5)] containing 1 μl of 10 mM ATP (R&D Systems, #EA004) in a final volume of 50 μl. All essential components for phosphorylation reaction were included in this system. A mix of 2 μM $Aβ_{1–42}$ alone in zymogen buffer with ATP was used as control group. The reaction of Aβ degradation was performed at 37°C for 10 hours and was stopped by cooling on ice for 5 min. The reaction was loaded into Biofuraw precast 4 to 12% bis-tris gel, and the remaining $Aβ_{1–42}$ was measured by quantitative Western blot analysis as described above.

Amyloid $β_{1–40}/_{1–42}$ ELISA

$Aβ_{1–40/1–42}$ concentrations were measured by using a human β-amyloid (1–42) ELISA kit (Wako, #298-62401) and a human β-amyloid (1–40) ELISA kit (Wako, #292-62301) according to the manufacturer′s instructions. For in vitro experiments, WT hippocampal neuronal cultures were transduced by AAV-CAG-EGFP and AAV-CAG-M7CK-EGFP (1 μl/1 ml of culture medium) virus at 7 DIV. After Aβ treatment at 12 DIV, the neuronal cultures were separated to four groups: EGFP or M7CK-EGFP with or without $Aβ_{1–42}$. At 14 DIV, neuronal culture medium (1 ml) was collected, and then neurons in the cultured slides were gently washed by PBS and collected as three neuronal cultures in one tube. Hippocampal neuronal cultures were homogenized in RIPA buffer (Beyotime, #P0013B) containing protease and phosphatase inhibitors, kept on ice for 20 min, and then centrifuged at 12,000 rpm for 10 min at 4°C to collect supernatant for Aβ ELISA. Total protein concentrations of neuronal homogenates were determined using the BCA kit (Thermo Fisher Scientific). *5XFAD* hippocampal neuronal cultures were transduced with AAV virus at 7 DIV, and culture medium was collected for Aβ ELISA at 14 DIV. Afterward, gradient $Aβ_{1–42}$ standard solutions were prepared, and 100 μl of diluted samples and standards was added into each well embedded with primary antibody, sealed, and kept overnight at 4°C. After washing, the wells were incubated with 100 μl of the HRP-conjugated antibody solution for 1 hour at 4°C followed by incubation with 100 μl of trimethylboron solution for 30 min at room temperature in the dark. After adding 100 μl of stop solution, the absorbance of each well was read at 450 nm with the microplate reader MultiScan Go. The $Aβ_{1–42}$ concentration for each sample was calculated according to standard curve.

The hippocampi of *5XFAD* mice overexpressing EGFP or M7CK-EGFP virus were homogenized in RIPA buffer with protease and phosphatase inhibitors, kept on ice for 20 min, and centrifuged at 12,000 rpm for 30 min at 4°C. The supernatant was collected to quantify the soluble Aβ. The sediment was resuspended in digestion buffer [5 M guanidine HCl in 50 mM tris (pH 8.0)] and centrifuged at 12,000 rpm for 30 min at 4°C. The supernatant was collected and used to quantify the insoluble part of Aβ. Both soluble and insoluble parts were subjected to Aβ measurement using a human β-amyloid (1–42) ELISA kit and a human β-amyloid (1–40) ELISA kit as mentioned above.

Aβ plaque immunostaining and quantification

After blocking with 5% goat serum, frozen sections that were mounted on slides were incubated with primary antibody for Aβ (1:1000; Cell Signaling Technology, #9888) overnight at 4°C in a humid chamber. After washing with PBS, sections were incubated with biotinylated secondary antibody for 30 min and VECTASTAIN ABC reagent (Vector Laboratories, #PK-4000) for 30 min at room temperature. Afterward, sections were incubated in peroxidase substrate chromogen 3,3′-diaminobenzidine (Sangon, #E670033) for 20 min at room temperature. Sections were rinsed by tap water gently to decrease background color. Stained sections were imaged by Olympus VS120 microscope with 10× objective lens at hippocampus. Aβ plaque density within hippocampus was analyzed by Image-Pro Plus 6.0. According to the preliminary experiment, brain sections of WT mice showed no Aβ plaque signal completely. For analysis, Aβ plaques were outlined manually until all plaques were included, and then the same parameters were applied to all images from both groups (*5XFAD* overexpressing EGFP or M7CK-EGFP in the hippocampus). The density of Aβ plaques in the hippocampus was measured from three sections per mouse.

Novel object recognition test

NORT was used to evaluate 24-hour memory in a 4-day session. The mice were allowed to explore freely for 10 min in an open-field apparatus (50 cm by 50 cm by 50 cm polyvinyl chloride arena with white walls and floor) on day 1 (″habituation phase″). The session was videotaped, and the videos were analyzed later for monitoring the exploration and locomotor activity of the mice by using Lime Light software (Coulbourn Instruments). On day 2, the mice were given another 5-min habituation phase in the same arena. On day 3, each mouse was placed into the open-field arena and exposed to four identical objects for 5 min (″sample phase″). Exploration counts toward each object were counted, and total exploration counts were used as a control for baseline exploration activity. Twenty-four hours after this sampling phase, the familiar object with the least exploration counts was substituted with a novel object at the same location, and mice were returned to the arena for 5 min of free exploration (″acquisition phase″) to assess memory. Videos from this acquisition phase were analyzed by at

least two experimenters. The recognition index was calculated as a percentage of exploration counts toward each object over all four objects, and the recognition index of novel object in comparison with that of the other three familiar objects (averaged together) was presented. Completely different objects were used for every experiment when NORT was performed at 6, 10, and 15 months of age.

Y-maze

The Y-maze test was used to assess spatial working memory functions. Each mouse was allowed to explore freely in a Y-shaped maze (arm length × width × height: 35 cm × 5 cm × 15 cm with three black opaque plastic arms at a 120° angle from each other) without any internal or external cues for 8 min. The session was videotaped. A spontaneous alternation was defined as successive entries into three different arms without repetition (such as ABC or BCA). A triad means that mice entered the three arms consecutively. The number of total entries into arms and the number of spontaneous alternations were assessed:

$$\text{Number of triads} = (\text{Total entries} - 2)$$

$$\text{Spontaneous alternation } (\%) = \frac{\#\text{ of Spontaneous alternations}}{\#\text{ of triads}} \times 100$$

Cognition wall spatial task

The cognition wall spatial task was performed as described previously (*16*). Mice were placed in the PhenoTyper cages (length × width × height: 30 cm × 30 cm × 35 cm, Noldus Information Technology, Netherlands) consisting of transparent walls with a white floor covered by standard bedding. Mice were allowed to habituate for 11 hours with free access to water but limited access to food before the task was commenced. Ten food pellets were given to each mouse in advance to help it locate the food dispenser. The task lasted for 13 hours in total (from 8:00 a.m. to 9:00 p.m.). The cognition wall includes three entry holes with one correct hole. One food pellet was given automatically by the food dispenser (Noldus) after every fifth correct hole entry during the task. The obtained food pellets and motion track of each mouse were recorded and analyzed automatically along the time period (EthoVision XT 12 software, Noldus). The mouse learned the task only when it reached the criteria of 80% correct hole entrance during the last 30 entries. The total entries until either the mice had learned the task or up to 13 hours (whichever came first) were recorded and used for analysis. The task automatically assessed the learning speed and the percentage of mice that had learned the task. The learning curve was plotted as a survival plot, with log-rank statistics. The consumed food pellets by each mouse were counted manually to confirm no errors with the food dispenser and automated read outs during the 13-hour session.

Nest construction test

Each mouse was housed individually 1 week before the test. Nest construction test was performed from 11:00 a.m. until 11:00 p.m. Before the task, each cage was covered with 5 cm–by–5 cm square tissue. Images were taken at the end of the test. Nesting behavior was scored following the rules: 5 = all tissue was torn into small pieces and gathered properly in a corner, 4 = most tissue was torn and gathered, 3 = some tissue was gathered and torn moderately, 2 = some tissue was torn but without gathering, and 1 = no tissue was torn or gathered.

Statistical analysis

All data were analyzed by GraphPad Prism (GraphPad). Data were first subjected to tests for normality and variance homogeneity (table S2). Shapiro-Wilk normality test was used to check whether the data were conforming to normal distribution. Variance homogeneity was assessed by F test for two-group experiments and evaluated by Brown-Forsythe test for multiple-group experiments. For two-group comparison, two-tailed unpaired t test was used for normally distributed data, unpaired t test with Welch's correction was used for data with uneven variance, and Mann Whitney test was used for data that were not normally distributed. For multigroup comparisons, one-way analysis of variance (ANOVA) was followed by Bonferroni's post hoc test with normally distributed data, or one-way ANOVA Kruskal-Wallis test was adopted followed by Dunn's post hoc with not normally distributed data. Experiments involving two factorial analyses were examined by using two-way ANOVA. For two-way ANOVA, Bonferroni's post hoc test was used for comparisons. Survival plot data were analyzed with log-rank statistics (Mantel-Cox test). All data are presented as mean ± SEM. Statistical significance was defined as $P < 0.05$. Also provided in the Supplementary Materials are tabulated details of the sample sizes (table S3) and statistical analysis information (table S4) for each dataset in this study.

Supplementary Materials

This PDF file includes:
Figs. S1 to S7
Tables S1 to S4

Other Supplementary Material for this manuscript includes the following:
Data files S1 and S2
MDAR Reproducibility Checklist

View/request a protocol for this paper from *Bio-protocol*.

REFERENCES AND NOTES

1. J. M. Long, D. M. Holtzman, Alzheimer disease: An update on pathobiology and treatment strategies. *Cell* **179**, 312–339 (2019).
2. G. S. Bloom, Amyloid-β and tau: The trigger and bullet in Alzheimer disease pathogenesis. *JAMA Neurol.* **71**, 505–508 (2014).
3. D. J. Selkoe, Alzheimer's disease is a synaptic failure. *Science* **298**, 789–791 (2002).
4. J. Hardy, D. J. Selkoe, The amyloid hypothesis of Alzheimer's disease: Progress and problems on the road to therapeutics. *Science* **297**, 353–356 (2002).
5. K. G. Mawuenyega, W. Sigurdson, V. Ovod, L. Munsell, T. Kasten, J. C. Morris, K. E. Yarasheski, R. J. Bateman, Decreased clearance of CNS β-amyloid in Alzheimer's disease. *Science* **330**, 1774 (2010).
6. D. J. Selkoe, J. Hardy, The amyloid hypothesis of Alzheimer's disease at 25 years. *EMBO Mol. Med.* **8**, 595–608 (2016).
7. G. M. Shankar, D. M. Walsh, Alzheimer's disease: Synaptic dysfunction and Aβ. *Mol. Neurodegener.* **4**, 48 (2009).
8. S. W. Scheff, D. A. Price, F. A. Schmitt, S. T. DeKosky, E. J. Mufson, Synaptic alterations in CA1 in mild Alzheimer disease and mild cognitive impairment. *Neurology* **68**, 1501–1508 (2007).

9. T. Saido, M. A. Leissring, Proteolytic degradation of amyloid β-protein. *Cold Spring Harb. Perspect. Med.* **2**, a006379 (2012).
10. T. Behl, G. Kaur, A. Sehgal, S. Bhardwaj, S. Singh, C. Buhas, C. Judea-Pusta, D. Uivarosan, M. A. Munteanu, S. Bungau, Multifaceted role of matrix metalloproteinases in neurodegenerative diseases: Pathophysiological and therapeutic perspectives. *Int. J. Mol. Sci.* **22**, 1413 (2021).
11. K. Kikuchi, T. Tatebe, Y. Sudo, M. Yokoyama, K. Kidana, Y. W. Chiu, S. Takatori, M. Arita, Y. Hori, T. Tomita, GPR120 signaling controls amyloid-β degrading activity of matrix metalloproteinases. *J. Neurosci.* **41**, 6173–6185 (2021).
12. N. A. Py, A. E. Bonnet, A. Bernard, Y. Marchalant, E. Charrat, F. Checler, M. Khrestchatisky, K. Baranger, S. Rivera, Differential spatio-temporal regulation of MMPs in the 5xFAD mouse model of Alzheimer's disease: Evidence for a pro-amyloidogenic role of MT1-MMP. *Front. Aging Neurosci.* **6**, 247 (2014).
13. M. J. Nadler, M. C. Hermosura, K. Inabe, A. L. Perraud, Q. Zhu, A. J. Stokes, T. Kurosaki, J. P. Kinet, R. Penner, A. M. Scharenberg, A. Fleig, LTRPC7 is a Mg.ATP-regulated divalent cation channel required for cell viability. *Nature* **411**, 590–595 (2001).
14. L. W. Runnels, L. Yue, D. E. Clapham, TRP-PLIK, a bifunctional protein with kinase and ion channel activities. *Science* **291**, 1043–1047 (2001).
15. G. Krapivinsky, L. Krapivinsky, Y. Manasian, D. E. Clapham, The TRPM7 chanzyme is cleaved to release a chromatin-modifying kinase. *Cell* **157**, 1061–1072 (2014).
16. Y. Liu, C. Chen, Y. Liu, W. Li, Z. Wang, Q. Sun, H. Zhou, X. Chen, Y. Yu, Y. Wang, N. Abumaria, TRPM7 is required for normal synapse density, learning, and memory at different developmental stages. *Cell Rep.* **23**, 3480–3491 (2018).
17. Y. Sun, P. Sukumaran, A. Schaar, B. B. Singh, TRPM7 and its role in neurodegenerative diseases. *Channels* **9**, 253–261 (2015).
18. M. C. Hermosura, H. Nayakanti, M. V. Dorovkov, F. R. Calderon, A. G. Ryazanov, D. S. Haymer, R. M. Garruto, A TRPM7 variant shows altered sensitivity to magnesium that may contribute to the pathogenesis of two Guamanian neurodegenerative disorders. *Proc. Natl. Acad. Sci. U.S.A.* **102**, 11510–11515 (2005).
19. H. G. Oh, Y. S. Chun, Y. Kim, S. H. Youn, S. Shin, M. K. Park, T. W. Kim, S. Chung, Modulation of transient receptor potential melastatin related 7 channel by presenilins. *Dev. Neurobiol.* **72**, 865–877 (2012).
20. N. Landman, S. Y. Jeong, S. Y. Shin, S. V. Voronov, G. Serban, M. S. Kang, M. K. Park, G. di Paolo, S. Chung, T. W. Kim, Presenilin mutations linked to familial Alzheimer's disease cause an imbalance in phosphatidylinositol 4,5-bisphosphate metabolism. *Proc. Natl. Acad. Sci. U.S.A.* **103**, 19524–19529 (2006).
21. H. G. Oh, S. Chung, Activation of transient receptor potential melastatin 7 (TRPM7) channel increases basal autophagy and reduces amyloid β-peptide. *Biochem. Biophys. Res. Commun.* **493**, 494–499 (2017).
22. G. Krapivinsky, S. Mochida, L. Krapivinsky, S. M. Cibulsky, D. E. Clapham, The TRPM7 ion channel functions in cholinergic synaptic vesicles and affects transmitter release. *Neuron* **52**, 485–496 (2006).
23. Z. J. Jiang, W. Li, L. H. Yao, B. Saed, Y. Rao, B. S. Grewe, A. McGinley, K. Varga, S. Alford, Y. S. Hu, L. W. Gong, TRPM7 is critical for short-term synaptic depression by regulating synaptic vesicle endocytosis. *eLife* **10**, e66709 (2021).
24. H. Oakley, S. L. Cole, S. Logan, E. Maus, P. Shao, J. Craft, A. Guillozet-Bongaarts, M. Ohno, J. Disterhoft, L. van Eldik, R. Berry, R. Vassar, Intraneuronal β-amyloid aggregates, neurodegeneration, and neuron loss in transgenic mice with five familial Alzheimer's disease mutations: Potential factors in amyloid plaque formation. *J. Neurosci.* **26**, 10129–10140 (2006).
25. J. L. Jankowsky, D. J. Fadale, J. Anderson, G. M. Xu, V. Gonzales, N. A. Jenkins, N. G. Copeland, M. K. Lee, L. H. Younkin, S. L. Wagner, S. G. Younkin, D. R. Borchelt, Mutant presenilins specifically elevate the levels of the 42 residue β-amyloid peptide in vivo: Evidence for augmentation of a 42-specific γ secretase. *Hum. Mol. Genet.* **13**, 159–170 (2004).
26. R. S. Reiserer, F. E. Harrison, D. C. Syverud, M. P. McDonald, Impaired spatial learning in the APP_{Swe} + PSEN1ΔE9 bigenic mouse model of Alzheimer's disease. *Genes Brain Behav.* **6**, 54–65 (2007).
27. J. W. Blanchard, L. A. Akay, J. Davila-Velderrain, D. von Maydell, H. Mathys, S. M. Davidson, A. Effenberger, C. Y. Chen, K. Maner-Smith, I. Hajjar, E. A. Ortlund, M. Bula, E. Agbas, A. Ng, X. Jiang, M. Kahn, C. Blanco-Duque, N. Lavoie, L. Liu, R. Reyes, Y. T. Lin, T. Ko, L. R'Bibo, W. T. Ralvenius, D. A. Bennett, H. P. Cam, M. Kellis, L. H. Tsai, APOE4 impairs myelination via cholesterol dysregulation in oligodendrocytes. *Nature* **611**, 769–779 (2022).
28. C. Ripoli, R. Piacentini, E. Riccardi, L. Leone, D. D. Li Puma, G. Bitan, C. Grassi, Effects of different amyloid β-protein analogues on synaptic function. *Neurobiol. Aging* **34**, 1032–1044 (2013).
29. M. Matsushita, J. A. Kozak, Y. Shimizu, D. T. McLachlin, H. Yamaguchi, F. Y. Wei, K. Tomizawa, H. Matsui, B. T. Chait, M. D. Cahalan, A. C. Nairn, Channel function is dissociated from the intrinsic kinase activity and autophosphorylation of TRPM7/ChaK1. *J. Biol. Chem.* **280**, 20793–20803 (2005).
30. B. N. Desai, G. Krapivinsky, B. Navarro, L. Krapivinsky, B. C. Carter, S. Febvay, M. Delling, A. Penumaka, I. S. Ramsey, Y. Manasian, D. E. Clapham, Cleavage of TRPM7 releases the kinase domain from the ion channel and regulates its participation in Fas-induced apoptosis. *Dev. Cell* **22**, 1149–1162 (2012).
31. V. Chubanov, K. P. Schlingmann, J. Wäring, J. Heinzinger, S. Kaske, S. Waldegger, M. M. Schnitzler, T. Gudermann, Hypomagnesemia with secondary hypocalcemia due to a missense mutation in the putative pore-forming region of TRPM6. *J. Biol. Chem.* **282**, 7656–7667 (2007).
32. M. Ruiter, L. J. Herstel, C. J. Wierenga, Reduction of dendritic inhibition in CA1 pyramidal neurons in amyloidosis models of early Alzheimer's disease. *J. Alzheimers Dis.* **78**, 951–964 (2020).
33. A. T. Barros-Viegas, V. Carmona, E. Ferreiro, J. Guedes, A. M. Cardoso, P. Cunha, L. P. de Almeida, C. R. de Oliveira, J. P. de Magalhães, J. Peça, A. L. Cardoso, miRNA-31 improves cognition and abolishes amyloid-β pathology by targeting APP and BACE1 in an animal model of Alzheimer's disease. *Mol. Ther. Nucleic Acids* **19**, 1219–1236 (2020).
34. F. M. Menzies, A. Fleming, A. Caricasole, C. F. Bento, S. P. Andrews, A. Ashkenazi, J. Füllgrabe, A. Jackson, M. Jimenez Sanchez, C. Karabiyik, F. Licitra, A. Lopez Ramirez, M. Pavel, C. Puri, M. Renna, T. Ricketts, L. Schlotawa, M. Vicinanza, H. Won, Y. Zhu, J. Skidmore, D. C. Rubinsztein, Autophagy and neurodegeneration: Pathogenic mechanisms and therapeutic opportunities. *Neuron* **93**, 1015–1034 (2017).
35. B. Boland, A. Kumar, S. Lee, F. M. Platt, J. Wegiel, W. H. Yu, R. A. Nixon, Autophagy induction and autophagosome clearance in neurons: Relationship to autophagic pathology in Alzheimer's disease. *J. Neurosci.* **28**, 6926–6937 (2008).
36. G. G. O. R. Grafinger, T. Stirling, M. I. Brasher, M. G. Coppolino, β1 integrin-mediated signaling regulates MT1-MMP phosphorylation to promote tumour cell invasion. *J. Cell Sci.* **133**, jcs239152 (2020).
37. E. Lagoutte, C. Villeneuve, L. Lafanechère, C. M. Wells, G. E. Jones, P. Chavrier, C. Rossé, LIMK regulates tumor-cell invasion and matrix degradation through tyrosine phosphorylation of MT1-MMP. *Sci. Rep.* **6**, 24925 (2016).
38. P. Yan, X. Hu, H. Song, K. Yin, R. J. Bateman, J. R. Cirrito, Q. Xiao, F. F. Hsu, J. W. Turk, J. Xu, C. Y. Hsu, D. M. Holtzman, J. M. Lee, Matrix metalloproteinase-9 degrades amyloid-beta fibrils in vitro and compact plaques in situ. *J. Biol. Chem.* **281**, 24566–24574 (2006).
39. A. E. Roher, T. C. Kasunic, A. S. Woods, R. J. Cotter, M. J. Ball, R. Fridman, Proteolysis of Aβ peptide from Alzheimer disease brain by gelatinase A. *Biochem. Biophys. Res. Commun.* **205**, 1755–1761 (1994).
40. L. V. Ryazanova, M. V. Dorovkov, A. Ansari, A. G. Ryazanov, Characterization of the protein kinase activity of TRPM7/ChaK1, a protein kinase fused to the transient receptor potential ion channel. *J. Biol. Chem.* **279**, 3708–3716 (2004).
41. M. J. Oentaryo, A. C. Tse, C. W. Lee, Neuronal MT1-MMP mediates ECM clearance and Lrp4 cleavage for agrin deposition and signaling in presynaptic development. *J. Cell Sci.* **133**, jcs246710 (2020).
42. M. Aarts, K. Iihara, W. L. Wei, Z. G. Xiong, M. Arundine, W. Cerwinski, J. F. MacDonald, M. Tymianski, A key role for TRPM7 channels in anoxic neuronal death. *Cell* **115**, 863–877 (2003).
43. H. Jiang, S. L. Tian, Y. Zeng, L. L. Li, J. Shi, TrkA pathway(s) is involved in regulation of TRPM7 expression in hippocampal neurons subjected to ischemic-reperfusion and oxygen-glucose deprivation. *Brain Res. Bull.* **76**, 124–130 (2008).
44. H. S. Sun, M. F. Jackson, L. J. Martin, K. Jansen, L. Teves, H. Cui, S. Kiyonaka, Y. Mori, M. Jones, J. P. Forder, T. E. Golde, B. A. Orser, J. F. MacDonald, M. Tymianski, Suppression of hippocampal TRPM7 protein prevents delayed neuronal death in brain ischemia. *Nat. Neurosci.* **12**, 1300–1307 (2009).
45. C. P. Yang, Z. H. Zhang, L. H. Zhang, H. C. Rui, Neuroprotective role of microRNA-22 in a 6-hydroxydopamine-induced cell model of Parkinson's disease via regulation of its target gene TRPM7. *J. Mol. Neurosci.* **60**, 445–452 (2016).
46. D. Erten-Lyons, A. Jacobson, P. Kramer, A. Grupe, J. Kaye, The *FAS* gene, brain volume, and disease progression in Alzheimer's disease. *Alzheimers Dement.* **6**, 118–124 (2010).
47. Z. Cai, S. Jitkaew, J. Zhao, H. C. Chiang, S. Choksi, J. Liu, Y. Ward, L. G. Wu, Z. G. Liu, Plasma membrane translocation of trimerized MLKL protein is required for TNF-induced necroptosis. *Nat. Cell Biol.* **16**, 55–65 (2014).
48. A. Caccamo, C. Branca, I. S. Piras, E. Ferreira, M. J. Huentelman, W. S. Liang, B. Readhead, J. T. Dudley, E. E. Spangenberg, K. N. Green, R. Belfiore, W. Winslow, S. Oddo, Necroptosis activation in Alzheimer's disease. *Nat. Neurosci.* **20**, 1236–1246 (2017).
49. Y. Zhao, J. Wang, H. Jiang, Z. Yu, X. Li, J. Shi, Following OGD/R, annexin 1 nuclear translocation and subsequent induction of apoptosis in neurons are assisted by myosin IIA in a TRPM7 kinase-dependent manner. *Mol. Neurobiol.* **51**, 729–742 (2015).
50. M. Ries, R. Loiola, U. N. Shah, S. M. Gentleman, E. Solito, M. Sastre, The anti-inflammatory annexin A1 induces the clearance and degradation of the amyloid-β peptide. *J. Neuroinflammation* **13**, 234 (2016).

51. Y. Zhao, T. Kiss, J. DelFavero, L. Li, X. Li, L. Zheng, J. Wang, C. Jiang, J. Shi, Z. Ungvari, A. Csiszar, X. A. Zhang, CD82-TRPM7-Numb signaling mediates age-related cognitive impairment. *Geroscience* **42**, 595–611 (2020).
52. K. Clark, M. Langeslag, B. van Leeuwen, L. Ran, A. G. Ryazanov, C. G. Figdor, W. H. Moolenaar, K. Jalink, F. N. van Leeuwen, TRPM7, a novel regulator of actomyosin contractility and cell adhesion. *EMBO J.* **25**, 290–301 (2006).
53. J. Middelbeek, K. Vrenken, D. Visser, E. Lasonder, J. Koster, K. Jalink, K. Clark, F. N. van Leeuwen, The TRPM7 interactome defines a cytoskeletal complex linked to neuroblastoma progression. *Eur. J. Cell Biol.* **95**, 465–474 (2016).
54. J. R. Bamburg, B. W. Bernstein, Actin dynamics and cofilin-actin rods in Alzheimer disease. *Cytoskeleton* **73**, 477–497 (2016).
55. K. Liu, S. H. Xu, Z. Chen, Q. X. Zeng, Z. J. Li, Z. M. Chen, TRPM7 overexpression enhances the cancer stem cell-like and metastatic phenotypes of lung cancer through modulation of the Hsp90α/uPA/MMP2 signaling pathway. *BMC Cancer* **18**, 1167 (2018).
56. X. Zhang, H. Zu, D. Zhao, K. Yang, S. Tian, X. Yu, F. Lu, B. Liu, X. Yu, B. Wang, W. Wang, S. Huang, Y. Wang, Z. Wang, Z. Zhang, Ion channel functional protein kinase TRPM7 regulates Mg ions to promote the osteoinduction of human osteoblast via PI3K pathway: In vitro simulation of the bone-repairing effect of Mg-based alloy implant. *Acta Biomater.* **63**, 369–382 (2017).
57. J. M. Paumier, N. A. Py, L. García-González, A. Bernard, D. Stephan, L. Louis, F. Checler, M. Khrestchatisky, K. Baranger, S. Rivera, Proamyloidogenic effects of membrane type 1 matrix metalloproteinase involve MMP-2 and BACE-1 activities, and the modulation of APP trafficking. *FASEB J.* **33**, 2910–2927 (2019).
58. H. Braak, E. Braak, Neuropathological stageing of Alzheimer-related changes. *Acta Neuropathol.* **82**, 239–259 (1991).
59. S. S. Mirra, A. Heyman, D. McKeel, S. M. Sumi, B. J. Crain, L. M. Brownlee, F. S. Vogel, J. P. Hughes, G. van Belle, L. Berg, The consortium to establish a registry for Alzheimer's Disease (CERAD). Part II. Standardization of the neuropathologic assessment of Alzheimer's disease. *Neurology* **41**, 479–486 (1991).

Acknowledgments: We thank the National Health and Disease Human Brain Tissue Resource Center (China Brain Bank, Zhejiang University School of Medicine) for providing human hippocampal tissue of controls and patients with AD. We also thank W. Wang and Y. Chen for the kind help with the *5XFAD* mice. **Funding:** This work was funded by the National Natural Science Foundation (NSF) of China (nos. 31970942 and 81573408 to N.A.), the Shanghai Municipal Science and Technology Major Project (no. 2018SHZDZX01), ZJ Lab, and the Shanghai Center for Brain Science and Brain-Inspired Technology. **Author contributions:** N.A. and W.L. conceived, designed, and supervised the project. S.Z. and F.C. conducted experiments and data analysis. All authors contributed to writing the manuscript. **Competing interests:** The authors declare a patent application submitted by Fudan University that covers the use of the M7CK fragment of TRPM7 in applications for AD therapy. **Data and materials availability:** All data needed to evaluate the conclusions in the paper are present in the paper or the Supplementary Materials.

Submitted 29 August 2022
Accepted 15 June 2023
Published 11 July 2023
10.1126/scisignal.ade6325

Science Signaling

TRPM7 kinase activity induces amyloid-# degradation to reverse synaptic and cognitive deficits in mouse models of Alzheimer's disease

Shimeng Zhang, Feifei Cao, Wei Li, and Nashat Abumaria

Sci. Signal., **16** (793), eade6325.
DOI: 10.1126/scisignal.ade6325

Editor's summary
The abundance of the dual-function ion channel and kinase TRPM7 is decreased in postmortem brain samples from patients with Alzheimer's disease (AD). Zhang *et al*. uncovered a pathological role for loss of TRPM7 in AD. In mice modeling amyloid-#–induced pathology, synapse formation and cognitive function were restored in aged mice and preserved in pre-symptomatic, younger mice upon overexpression of the kinase portion of TRPM7 (called M7CK). M7CK directly activated the protease MMP14, which promoted amyloid-# degradation and clearance. The findings may provide a mechanistic link between TRPM7 loss and amyloid pathology in AD patients.–Leslie K. Ferrarelli

Science Signaling (ISSN) is published by the American Association for the Advancement of Science. 1200 New York Avenue NW, Washington, DC 20005. The title *Science Signaling* is a registered trademark of AAAS.